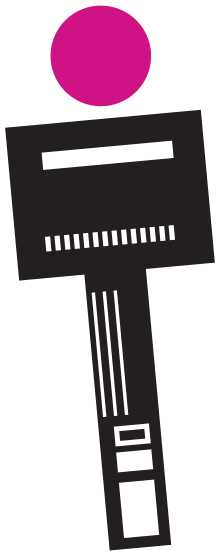

RAM ROBOTICS AND MECHATRONICS

DEVELOPMENT AND IMPLEMENTATION OF AN MR-SAFE ENCODER FOR PNEUMATIC ACTUATORS OF THE MR-SAFE CATHETER ROBOT FOR ENDOVASCULAR APPLICATIONS

N.B. (Niek) Morsinkhof

MSC ASSIGNMENT

Committee:
prof. dr. ir. S. Stramigioli
dr. G. Dagnino
dr. V. Groenhuis, MSc
dr. ir. R.W. van Delden

January, 2022

003RaM2022
Robotics and Mechatronics
EEMathCS
University of Twente
P.O. Box 217
7500 AE Enschede
The Netherlands

UNIVERSITY OF TWENTE. | TECHMED CENTRE UNIVERSITY OF TWENTE. | DIGITAL SOCIETY INSTITUTE

Summary

Endovascular procedures can be a challenging and delicate task for surgeons. Surgeons have to rely on 2d-imaging and relative small forces and torques to manoeuvre a catheter through the blood vessel. Also fluoroscopy is used as an imaging technique which can be harmful for medical personnel which performs these operations frequently. To circumvent these problems a tele-manipulative robotic sytem has been developed, which enables surgeons to operate remotely, without being exposed to health risks due to fluoroscopy. The platform also features a navigation system that provides the surgeons with visual and haptic guidance during the procedure.

The actuators of the secondary robot, which move the catheter and guidewire, are pneumatically driven and fully made of MR-safe materials, enabling the secondary robot to be MR-safe. Both the rotary and linear actuators move the catheter in distinct steps. A limitation of the current prototype is that it lacks any positional feedback from the actuators. Occasionally there is a loss of pressure in the piston chamber of the actuator, which causes a reduced force output, therefore it may occur that the actuator misses steps. To compensate for these errors, a feedback system is required to improve the reliability and robustness of the system.

To achieve feedback from the actuators, an MR-safe sinusoidal encoding method is proposed. In the proposed method optic fibers are used together with a grating pattern from MR-safe material to create periodic analog signals. The method is split into two basic concepts to achieve the desired resolution. In the first concept, the linear movement of the actuator is translated to an angular movement such that the size of the grating pattern can be increased. Subsequently, two optic fibers are used to create an analog encoding signal. In the second concept, three analog signals are created by three cables and a grating pattern of which the grating period is six times the desired resolution. Three optic fibers and a grating pattern create three analog signals such that one grating period can be divided into six sections with the length of the desired resolution.

The tests proved that the accuracy of the encoders was satisfactory. The precision of both encoders was relatively low, which caused measurement deficiencies. The first concept clearly had more measurement complications, caused by a too low sampling frequency and mechanical problems such as the rotation of the motor-housing. The second concept has still a too low precision, which is caused by a poor analog signal. In future works it is recommended to further develop the second design, which includes improving the analog signal of the second design, and create an adequate alignment of the encoder with respect to the static motor locations.

Preface

The work that is written in this thesis is to conclude the Master of Science programme in Electrical Engineering within the Robotic and Mechatronics group (RaM) at the University of Twente.

Firstly, I want to thank Dr.ir. Giulio Dagnino for his guidance throughout the project. Secondly, I would like to thank Dr. Vincent Groenhuis, for giving direction during the project, especially regarding the technical technical aspects of the project. Finally, I would like to thank Ing. Sander Smits for providing feedback on the CAD-designs and printing a large parts of my prototypes.

Contents

1 Introduction

1.1 Context

Over the last decades, deaths and disability due to cardiovascular diseases have been on the rise worldwide. In 2019 alone, one-third of all deaths could be attributed to cardiovascular diseases[1]. Important examples of cardiovascular conditions are atherosclerosis, aneurysmal artial disease, and cardiac arythmias [2]. Atherosclerosis occurs when atheromatous plaque builds up inside the artery, reducing the blood flow. This can have far-reaching consequences such as heart attacks or strokes. Another serious cardiovascular condition is aneurysmal artial disease, which is caused by a weak spot of the artial wall. The weak spot can lead to an outward bulging, which can be deadly in the case of a rupture. One more cardiovascular condition is cardiac arythmias which corresponds to an abnormal heart rate.

The development of minimally invasive endovascular surgery, paved the way for an alternative to open surgery techniques. The advancement of endovascular surgery has revolutionized diagnosis and management of cardiovascular disease in almost every way[3]. Endovascular interventions involves the insertion and manipulation of a catheter and guidewire into the vascular system. Intra-operative visual guidance is usually provided by fluoroscopy, where a contrast agent is injected into the vascular system to visualise the vessels. One example of such an endovascular intervention is the expansion of an inflatable balloon within the vessel. this procedure, which is called percutaneous tansluminal angioplasty, is performed in order to compact atheromatous plaque or to open up stenosis. Another example is the treatment of aneurysm, where a stent is deployed at the location of the aneurysm such that the pressure exerted on the weakened aneurysm wall is released[2].

The manual performance of an endovascular intervention can be a challenging process. The surgical operator has to rely on the 2d-imaging and on relatively small forces and torques due to contact at the end of the catheter. An additional challenge of an enodvascular operation is the use of X-ray fluoroscopy where the surgical operator is exposed to cumulative doses of radiation which, in long-term, may lead to an increased chance of cancer[4]. A study of Ho et al[5], to the effects of percutaneous coronary interventions on the risk of cancer among cardiologists, concludes that cardiologist who frequently perform percutaneous coronary interventions have a higher risk of cancer.

In the light of these challenges tele-robotic technology has been introduced to assist with endovascular interventions. A tele-robotic system is a system that is remotely controlled by a human operator. There are two main components that form the basis of the tele-robotic system, the master device and the secondary device. The master device is the part of the tele-robotic system that interfaces with the human operator. According to the interface input given by the human operator, the secondary device of the tele-robotic system is controlled remotely. To overcome the human limitations and risks regarding X-ray fluoroscopy, tele-robotic systems have been introduced in the form of robotic steerable catheter technology. The technology has proven to enhance precision and stability, reduce radiation doses, and improve access to difficult anatomy[6].

Despite the contributions tele-robotics systems have provided for endovascular interventions, there are still shortcomings to the technology. These include a lack of haptic feedback, and an excessive amount of radiation to the patient[7]. A novel master-slave robotic platform(fig 1.1) has been proposed which implements haptic-feedback to the master platform. The master-platform has an intuitive user interface such that it provides a clinical familiar workflow. The secondary platform of the tele-robotic system is fully fabricated with additive manufacturing which enables the secondary platform to be MR-compatible.

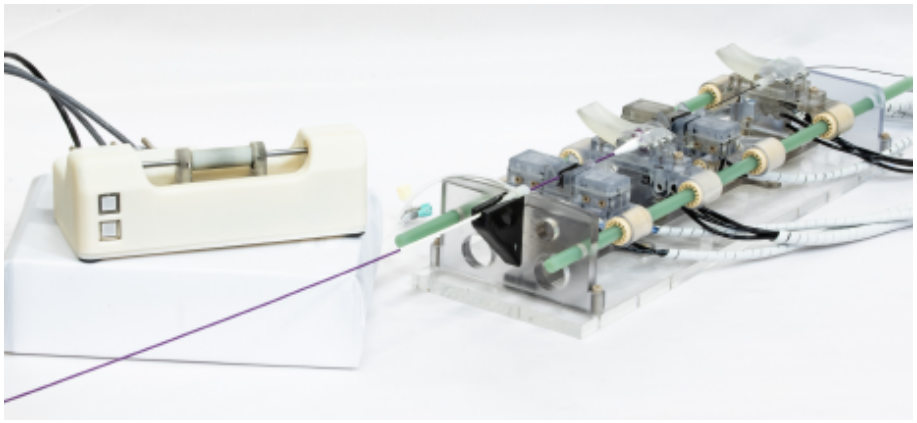

Figure 1.1: Prototype of the CathBot tele-robotic system[7]. The master part can be seen on the left, the secondary part on the right.

The secondary platform of the CathBot is able to manipulate catheters and guidewires.The catheters and guidewires are manipulated with pneumatic actuators. During the procedure the surgical operator receives vision-based haptic feedback in the form of viscious frictions which are rendered in the master manipulator proportionally to the instrument-vessel distance minimising endothelial damages to the vessel wall[7].

Currently there are no sensors integrated into the secondary part of the robot in order to retrieve data regarding the state of the pneumatic actuators.

1.2 Goals

The current design solely incorporates feedback from imaging. However, the system does not take into account any state information from its pneumatic actuators of the secondary part. These rotatory, linear and clamping actuators manipulate the catheters and guidewires, which are powered by an air compressor connected by relative long tubes. This actuation method occasionally causes the motor to miss steps.

The current system controls the state of the actuators based on open-loop control, which means that the state of the actuator is based on user inputs only and is moved to its desired state accordingly. If, however, a pneumatic actuator of the secondary device misses a step, the actual state of the actuator differs from the estimated state based on user input. Since estimating the state of the actuator based on the input from the master device is not 100% accurate, a feedback system is required in order to enable closed-loop control and have robust positioning of the actuator.

This assignment focuses on the design and implementation of MR-safe encoders for the actuators in the secondary part of the of the robotic system. These encoders will provide state information from the actuators, such that closed-loop control can be implemented in order to position the actuators. The assignment includes the following goals:

- Rebuild the secondary part of the prototype in fig 1.1
- Design an MR-safe rotary and linear encoder with the desired resolution
- Implement the encoder-designs into the prototype

Since an essential technical characteristic of the secondary part of the robotic platform is that it is MR-safe, the implementation of an encoder into the secondary part should affect this characteristic. Therefore, it is important that the encoder will be MR-safe too. The linear pneumatic

actuators from the secondary part of the robot, move in distinct steps and do not move continuously. The nominal stepsize of the linear pneumatic actuators is 0.3mm, which means that the resolution of the encoder has to conform to this measure to detect these steps. To guarantee a robust closed-loop control system it is also important to the precision of the encoder is sufficient. A lack in precision may lead to too much uncertainty in the measurements, and cause the encoder to miss steps. From this it can be stated that there are three important requirements for the encoder:

- The encoder should be MR-safe.
- The encoder should have a resolution which is high enough to detect steps of 0.3mm from the pneumatic actuator.
- The precision of the encoder should be such that the encoder does not miss any steps.

The optimal goal of this research is to realize an encoder which, while implemented in the CathBot prototype, meets these requirements. If not realized, this research should give at least sufficient insight in how to develop an encoder which has the mentioned requirements. The purpose of this research, to create an encoder with the above requirements, is described with the following research question.
How can an sufficiently accurate and precise MR-safe encoder be developed for the pneumatic actuators in the CathBot prototype in order to be able to realize a robust closed-loop feedback system?

The main research question will be broken down into the following subquestions:

- How reliable are the different designs concerning accuracy and precision of their measurements? Do they meet the demanding accuracy and precision such that the design is fully reliable?
- If there is a lack in precision and accuracy, What is the potential of the different designs to overcome this lack? How can the demands be met in future development?
- How do different designs of an MR-safe encoder conform to robustness regarding implementation? Does the design perform consistently?
- How feasible are the different designs concerning fabrication?

1.3 Outline

In chapter two, background information will be provided regarding endovascular conditions, interventions, and the development of tele-robotics in this field. Additionally, theory concerning optical and sinusoidal encoding will be given.

Chapter three will give an oversight in the development of the encoder-concepts and the corresponding testing of each design. In chapter four these results will be collected to a general oversight regarding the results of the different concepts.

In chapter five, the results will be discussed. It will be discussed what the tests have demonstrated regarding the research questions and future recommendations will be given concerning further development. In chapter six the results will be summarized by answering the research question.

2 Background

2.1 Cardiovascular diseases

Atherosclerosis is a condition where the arterial wall of the major conduit arteries are affected. The build-up of lipids called plaque, and oxidation can cause chronic inflammation which ultimately causes trombosisor stenosis[8]. Also the plaque can be freed from the vascular wall, and subsequently block the arterial system on a different location. This can lead to ischemia, or even to a heart attack or stroke. There are multiple factors that provoke atherosclerosis. This can be lifestyle related factors such as smoking, obesity, diabetes, or frequently hypertension due to stress, but also genetic predisposition can be the origin.

Another example of a vascular disease is aneurysm, where a weakened spot in the vascular wall leads to a bulging of that particularly part of the artery. Aneurysms can occur in any part of the vascular system, and are especially trheatingen when occuring in the coronary arteries, or brain arteries. The incidence of coronary aneurysms vaires from 1.5% to 5%[9]. In general the right coronary artery is most commonly involved in the disease followed by the left anterior descending artery[9].

Arrhythmia is a cardiovascular disease that can be life threatening too, or cause at least significant health problems. A heart arrhythmia is known as a heart condition where the heartbeat is irregular. This is caused by a deficiency in the electrical signals that coordinate the heart beat, such that the frequency of the heartbeat is irregularly, too fast, or too slow. A review study from 2008[10] concludes that experimental and epidemiological studies strongly suggest that cardiac arrhythmia is closely linked to hypertension.

2.2 Endovascular Interventions

Endovascular surgery is, contrary to open surgery, a less invasive procedure to treat cardiovascular diseases. Due to developments of endovascular interventions and in imaging technologies such as angioscopy and ultrasound many existing open operative procedures could be replaced by minimally invasive interventions[11].

Stenting
An endovascular intervention that is commonly used is the implantation of stents into the blood vessel. A stent is a metal or plastic tube and its function is to keep the vessel open such that a sufficient blood flow is maintained, or to reinforce the vessel wall. Examples of different types of stenting are[12], endovascular aneurysm repair, coronary artery stenting, peripheral artery stenting, and cerebral stenting.

The treatment of aneurysm with stent grafts is called endovascular aneurysm repair(EVAR). During an EVAR a small insision is made in the grion, subsequently a stent graft is inserted into the aneurysm through this incision[13]. A common complication of EVAR are endoleaks. An endoleak is defined as a blood flow outside the sten-graft, which occurs within the aneurysm sac[14]. Approximately 20% of the patients suffer from an endoleak after an EVAR[15].

Peripheral artery diseases is a vascular condition which develop in the limbs of the patient. Compared to percutaneous transluminal angioplasty, stenting has proven to have lower rates of restenosis[12]. The problem with peripheral artery stenting is that because arteries in the peripheral system are bounded by powerful muscles, there is a relative high risk for stent fracture[16]. The choice to perform this procedure should thus be based on the location of the specific peripheral artery.

Embolisation
In case of a threatening bleeding, caused by e.g. trauma, infections or blood clotting disor-

ders, a minimally invasive treatment called embolisation can be used, which is a treatment that blocks the affected vessel to stop the bleeding. The procedure is done by delivering embolic agents to the location of the bleeding. Different embolic agents can be used such as, gelatin sponge, polyvinyl alcohol, particles and metallic coils[17]. Applications of endovascular embolisation can be categorised in vascular, bleeding, oncology, women's health, men's health, and obesity[12].

An example of a vascular embolisation is endovascular coiling to treat ruptured cerbral aneurysms. A cerebral aneurysm is a weak spot in a vessel located in the brain which causes the vessel to bulge. The treatment is considered as an alternative to surgical clipping, since it is able to eliminate craniotomy, it can reduce damages to patients and accelerate recovery [18].

Ablation
Arrhythmia's caused by abnormal electrical signals can be treated by creating tiny scars in order to remove electrical pathways that cause these abnormal electrical signals. Electrode catheter are often inserted pecutaneously into the femoral veins and orientated within the heart to allow pacing stimulation[19]. Serious complications are uncommon for ablation interventions with a 0.05-0.01% stroke rate and heart block requiring a permanent pacemaker occurs in 0.5% of the cases[19].

2.3 Current Robot-assisted MR-safe Technology

Although minimally invasive endovascular interventions have proven to enhance the overall quality regarding the treatment and recovery of the patient, there are still limitations to overcome[2]. Due to fluoroscopy the surgeon is exposed to a significant dose of radiation which can be harmful after frequent exposure. Furthermore the surgeon is often restricted to 2d-imaging, and the contact force sensed from the vascular anatomy is limited.

Tele-robotic systems have been introduced to increase the sensorimotor capacity of humans behond the natural competence to achieve an augmented sensorimotor ability, which allows humans to interact with objects and environments remotely[20]. The implementation of telerobotic systems also provides a solution for the health risks associated with fluoroscopy, since tele-operation allows to manipulate devices in MRI environments, which also allows for high quality image feedback[21].

At present, different projects have successfully resulted in MR-guided telemanipulated robotic systems for endovascular proceducres [22]. But other surgical applications too, such as prostate interventions[23], bone biopsy [24], and general purpose needle guiding [25].

The tele-manipulated robotic system from Lee et al [22] uses continues hydraulic based actuator. The advantage of this design with respect to a pneumatically driven stepper motor is that it is capable of continues and torque-controllable rotary actuation. All the components of the secondary part of the robotic system where made MR-safe and most components where 3d-printed. A possible disadvantage of the design is that the maximum output forces and torques are limited by the mechanical strength of the 3d-printed components.

The MIRIAM robot from Moreira et al [23] uses piezoelectric and pneumatic actuation to move the needle with 9dof, which makes the design MR-conditional. The needle-guide robot from[] uses the pneumatic stepper motors from Stoianovici et al[26] to guarantee the MR-safe characteristic of the robot.
[27]

A study about the status and future trends regarding medical tele-robotic systems from [28], discusses issues regarding the adoption of tele-robotic technology in clinical practice. According to the study, one important issue are the high development costs related to the safety and reliability requirements of the regulatory systems. It is argued that, for an effective development process, the involvement of surgeons during the development is crucial. Effective inter-

action between the surgeon robotic technology is a critical component to ensure secure, more applicable, and adequate devices.

2.4 The CathBot Prototype and its Operating Principle

This project revolves around a Remote Tele-manipulative(fig. 1.1) system which purpose is to allow a surgical operator to perform endovascular procedures to reduce operating time, hospitalization, and recovery time. An important feature of the robotic system is the MR-safe characteristic of the secondary platform, which enables MR imaging, as a replacement of fluoroscopic imaging. This eliminates the negative side effects of the exposure to radiation and provides structural and functional soft tissue information such as the vasculature, at a high spatial resolution and contrast[29].

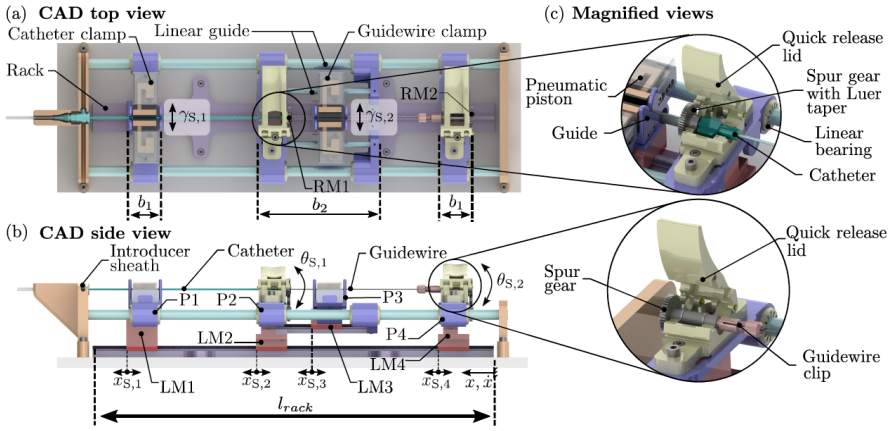

Figure 2.1: Conceptual design of the secondary part of the CathBot. [7]

In figure 2.1 it can be seen that different parts of the model are indicated with abbreviations that can be defined as follows [7]:

- Catheter platform 1(P1): linear motor 1(LM1)
- Catheter following/rotation platform(P2): Linear stepper motor (LM2) carrying a rotary stepper motor(RM1), a catheter hub docking station, and a guidewire feeding platform(P3)
- Guidewire feeding platform(P3): Linear stepper motor(LM3) carryig two J-clamps
- Guidewire following/rotation platform(p4): Linear stpper motor(LM4) carrying a rotary stepper motor(RM2) and a guidewire torque device docking station.

The master device takes input from the surgical operator by means of ergonomic interfacing, subsequently this input is translated into a desired actuation on the side of the secondary device. The secondary device is able to manipulate angiographic catheters and guidewires, with two linear actuator, one rotary actuator and two clamps for each instrument. To preserve the MR-safe property of the secondary device, the actuation is achieved by means of pneumatic stepper motors and clamps. Haptic feedback to the master device is generated through MRI-imaging. The clinical operator senses a viscous friction which is proportional to the distance of the distance from instrument to vessel-wall[7].

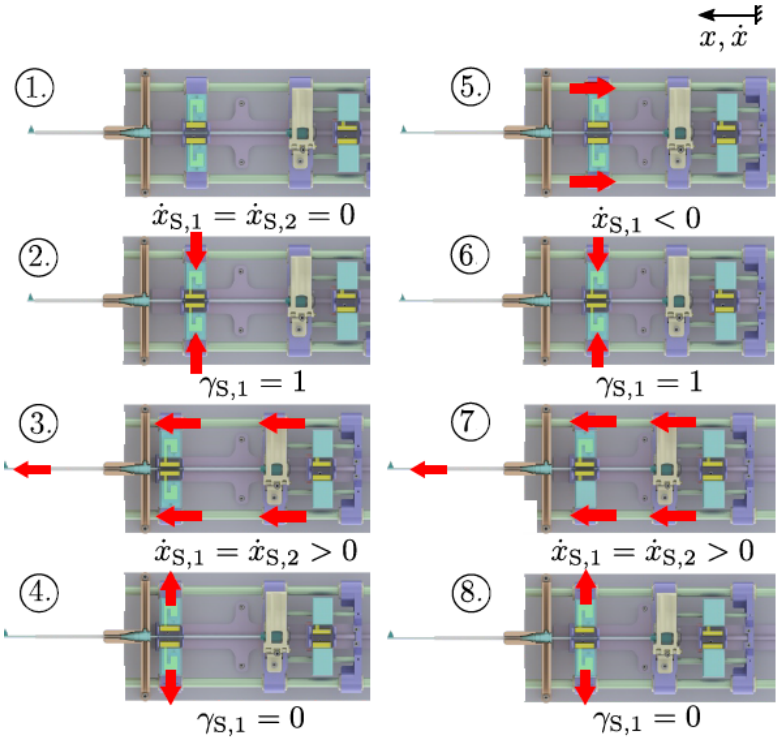

Figure 2.2: Example of insertion sequence[7]

In figure 2.2 an illustration is given of the sequence for a catheter insertion. The steps represents the following procedures [7]: (1) Starting from the initial static position, (2) P1 clamps the catheter. (3) P1 and P2 move at the same speed (to avoid buckling) and for the same predefined entire stroke. (4) P1 releases the catheter and returns to the initial position, (5) while P2 stays still. (6) P1 clamps the catheter again. (7) P1 and P2 advance simultaneously half of the defined stroke. (8) P1 releases the catheter.

2.5 Pneumatic actuators

The pneumatic actuators used in the prototype are based on the design of pneumatic actuators with double acting cylinders from V. Groenhuis[30] [31]. In figure 2.3 a schematic with its coherent realization can be seen of a pneumatic double-acting cylinder can be seen. From this figure one can perceive that the piston can be moved by consecutively pressurizing and depressurizing the two piston chambers. Alternating between pressurizing a chamber and releasing air from the chamber is done by means of a valves, such that when one chamber is pressurized, the other chamber is able to release air and vice-versa in order to move the piston in the opposite direction.

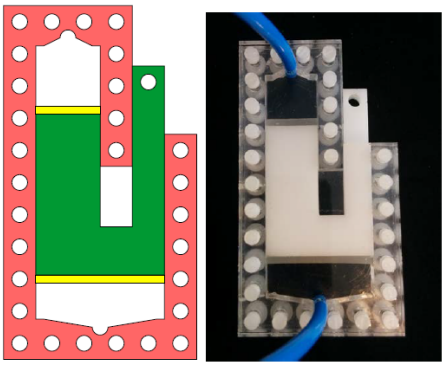

(a) Top view of design (b) Realization

Figure 2.3: Schematic and realization of a double-acting piston

Actuation is realized by means of teeth moving coherent with the piston, which grip inside a teeth-rack. In figure 2.4 a schematic can be seen which shows the principle of actuation according to 4 subsequent steps. From this schematic it can be observed that two pistons equipped with teeth generate a movement along the rack by alternating up and down. The two pistons have a relative phase-shift of 90°, hence the two pistons should be controlled according to a quadrature signal.

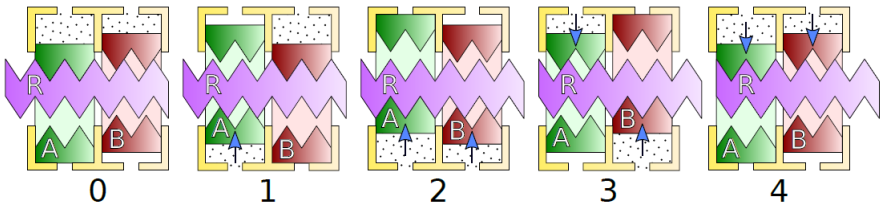

Figure 2.4: Schematic that illustrates the working principle of the pneumatic stepper motors which are used in the CathBot. For every step the motor moves with one-fourth of the teeth-pitch along the purple rack.

2.6 Operation of Sinusoidal Encoders

Sinusoidal encoders are used to track relative displacement of a particular component. An analog sinusoidal quadrature signal is generated by the sensor, proportional to this displacement, that may be based on capacitive, optical, inductive, hall-effect or magneto-electric principles[32].

To divide the one period of the analog quadratue signal into 4 sections, the analog quadrature signal can be converted into a logical block wave by applying a comparator or a threshold to the analog signal. In this fashion, one period has 4 distinct sections of equal lengths(see figure 2.5), provided that the two analog signals are perfect sine waves with a relative phase shift of exactly 90°.

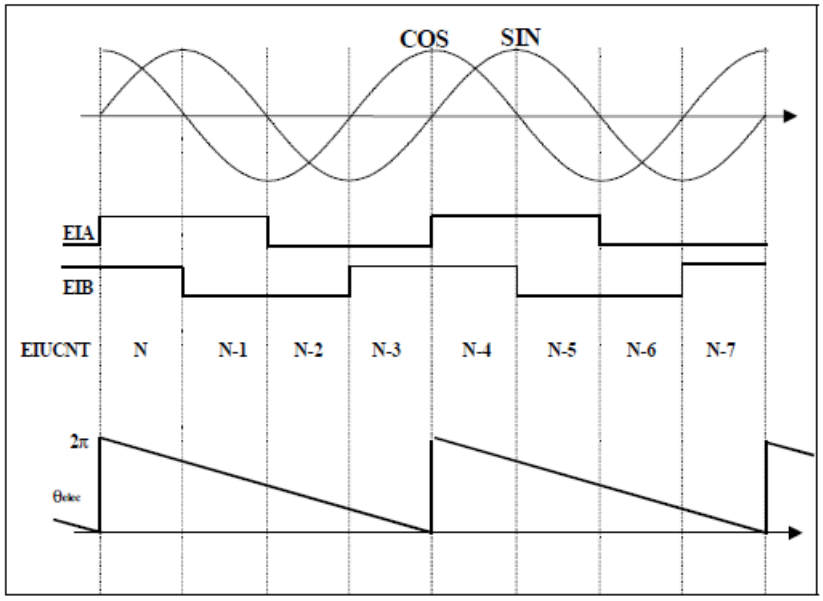

Figure 2.5: Schematic illustrating a quadrature signal, analog on top, logic in the middle, angular position below.

In case that the two analog signals have exactly the same amplitude, amplitude offset and the phase offset between the signals is 120°, the angle of the analog sinusoidal signal can easily be determined by means of [33]. When the analog signals can be described as a function of the angle$\theta(x)$, the position can determined accurately by applying the arctan function. When the two analog signals are described as follows, where x is the displacement that is to be determined by the encoder,

$$S_1 = A\sin\theta(x), \tag{2.1}$$
$$S_2 = A\cos\theta(x). \tag{2.2}$$

The angle $\theta(x)$ in one grating period can be determined,

$$\theta(x) = \arctan\left(\frac{S_1}{S_2}\right). \tag{2.3}$$

Errors

The analog signal originating from the sensor is never a perfect quadrature signal. The two signals may have a phase-shift which is not exactly 90°, The amplitude of the two signals can vary or the signals could have a different offset. These imbalances can be caused by inaccuracies in the manufacturing process. So instead of 2.1 and 2.2, the analog signal from the sensor is more likely to be described as follows[34],

$$S_1 = A\sin\theta(x) + V_{dc1},$$
$$S_2 = A(1+\alpha)\cos(\theta(x)+\delta) + V_{dc2}.$$

Where α and δ represent possible phase differences, and V_{dc1} V_{dc2} represent possible offsets in the analog signal. These imbalances could be eliminated by calibrating the sensors. In order to do this one could measure and average the imbalances, such that they can be subtracted from the original signal. It may also be the case that the imbalance is a periodic function of the

position, the analog signal can be represented by a Fourier series such that the coefficient that describes the imbalance as a function of the distance can be removed[35].

2.7 MR-safe Encoding with Fiber Optics

To measure the state of the linear and rotary actuators, sensors have to be implemented that guarantee the MR compatibility. In order to guarantee the MR compatibility of the system, encoding will be done by means of fiber optics which already has been proven to be a solid MR-safe encoding method [26] [36], but also reflective sensors have been used[37]. A fiberoptic cable will carry a light signal to the binary encoding patter, after which an fiber-optic cable at the other side of the encoding pattern will receive the light from the other cable.

There are two distinctive types of optical fibers, multimode and singlemode cables. Multimode cables have a larger diameter, typically 62.5μm core diameter, which allows the propagation of multiple light-modes. Because of the large diameter of the core, the cable is able to gather more light such that a simple LED can be used as light input source. In communication applications, the disadvantage of a large core-diameter is a reduced bandwidth-distance product, hence multimode fibers are typically used in small-distance communication.

A single-mode fiber typically has a smaller core diameter of 12.μm, such that only one mode can be transmitted. To drive a single-mode fiber it is not possible to use a simple LED, but a laser is required. The advantage of the smaller core diameter is that it enables single-core cables to be used for communication over larger distances.

In order to transmit light from the source fiber into the receiver fiber, the cables have to be aligned properly. Since the light at the output of the source fiber is divergent according to the refractive index of the cable, the spacing between the source and receiver fiber should be within range and often a collimator lens is used [38] to optimize a the free-space coupling.

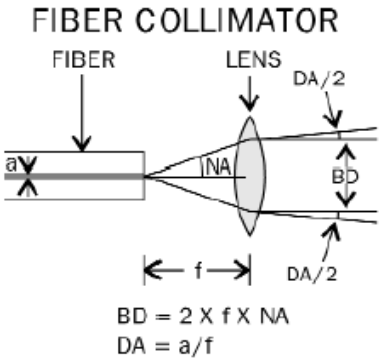

Figure 2.6: Operating principle of a fiber collimator[38]. The light from the source cable divergers according to the refractive index, and is subsequently focused by the lens in order for the receiving fiber to receive more light

3 Methods

3.1 Introduction

In order to determine how an MR-safe encoder for the pneumatic actuators in the CathBot-prototype can be realized, different concepts will be developed and tested.

Initially two concepts are proposed. In the first concept the linear movement of the motor will be translated into an angular movement, such that the linear stepsize is translated to an angular stepsize. Subsequently, the angular stepsize is transformed back to a linear stepsize that is proportional to the distance from the axis of rotation to the grating in the rotary component. In this manner, the grating period can be stretched out over a larger distance. The designs of this concept will be referred to as Rotary Encoder I and II.

The other concept will utilize the principle of three out of phase signals on the grating, such that the location on the grating period can be determined. With this concept, one grating period can be divided into 6 sections such that the required resolution can be met. The design of this concept will be referred to as 3-Phase Linear Encoder.

The methods will first be tested without implementation of the pneumatic motors. Before implementation, the concepts have to be verified upon their ability to detect steps of the required resolution, additionally there measurement accuracy will be tested. This first test will thus be done with a continues movement without the pneumatic motor. After this, the designs may be improved based on this first measurement and the next iteration will be tested with pneumatic motor.

To discern between the designs which are suitable for the CathBot and the designs which are less suitable for the CathBot the designs have to be tested such that they can be reflected upon the sub-research questions of this project. In this section different tests must be done to acquire data which can give a clear insight into the sub-questions. It is important that the tests precisely answer the following questions:

1. Precision: How does the actual nominal measured stepsize of the encoder conform to the expected measured stepsize of the encoder?
2. Accuracy: What is the accuracy of the measured stepsize?
3. Further development: If the design performs inadequate regarding points 1 and/or 2, what is the cause of this inadequacy? Which possible solutions will resolve these inadequacy?
4. Does the design perform consistently? Or does it have unpredictable behaviour? Can this be resolved?

When all test have been completed, a final evaluation will be done on the different concepts. In this evaluation the designs will be assessed based on the sub-questions which will eventually form the foundation of the research question of this project.

3.2 Assembly linear motors

A crucial part of the project to test the encoder designs are the linear pneumatic motors that will be used in the project. The motors will be printed with the objet 260, partly VeroWhite and partly VeroClear. The linear motor, see figure 3.2 consists in total out of 4 parts: The housing, the caps, the seals, and the pistons. The seals where lasercutted from 0.5mm siliconsheet, with dimensions 10.40mmx12.10mm. Before the pistons were placed inside the housing, the pistons were sanded to make sure the piston would move without to much resistance through the

housing. Since after printing the pistons, there would often be extra redundant material at the bottom of the piston. After the motor is fully assembled, it is important that enough pressure is built up to move the piston with sufficient force. Often a test was done by placing the cap on the housing on top first before glueing the cap on top, such that the a piston could always be replaced when there was too much resistance because of a slightly deformed piston. After this the caps were glued on top of the housing with Pattex super glue. The glueing should be done delicately and the caps should be fixed while drying. If the caps are placed on top too loosely their may be too much space between the piston and the caps such that there will be too much pressure loss. The pressure will will already be affected when the cap is placed a tenth of a millimeter too high, and if this is not done with care the whole 3d-printing process has to start over. During the assembly the original design of the motor was changed for three reasons. 1) in order to have more contact surface between the cap and the housing to glue them togheter. 2) In order to strengthen the cap, such that the cap will not break due to pressure build up. During previous test the original cap design would occasionally break due to pressure build up. 3) to make the linear motor compatible with the encoder.

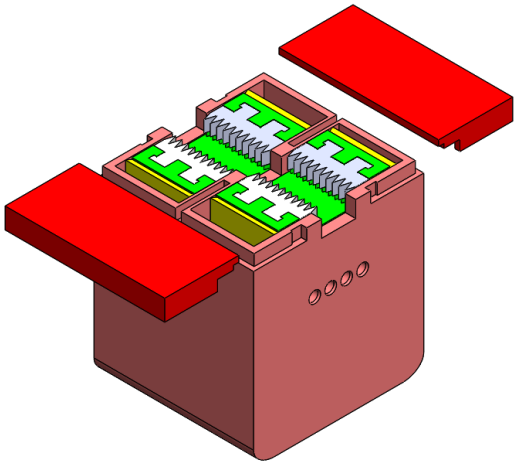

Figure 3.1: Exploded view of the original linear motor design for the CathBot. In the figure the housing(pink), the caps(red), the pistons(green/white) and the seals(yellow) are depicted.

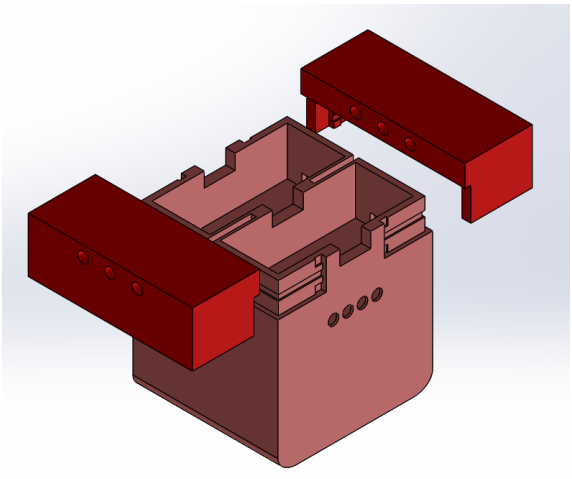

Figure 3.2: Exploded view of the redesigned linear motor housing and cap for the CathBot with encoder. The caps are strengthened and there is more surface for the glue to attach the cap to the housing.

3.3 Optical Circuit

To establish an optical circuit that is needed in this research, a light source for the optical fiber is required, a sensor is required to detect the light at the end of the fiber, and an amplification of the sensor output is required to be able to read output of the sensor.

In order to have a sufficiently strong optical signal at the end of the fiber such that it is detectable by a photo-transistor or photo-diode, a LED can be used with an adequate luminosity. Also, since the input of the cable is placed above the LED a low angle of half intensity is desirable. In this project the TLCR5800 ultrabright LED is used with a typical wavelength of 616nm, a typical luminosity of 35 cd and an angle of half intensity of 4 degrees.

To detect the light at the end of the fiber the EPM-4001 photo-diode is used. The sensor is matched to 660nm emitters, which sufficiently close to the 616nm wavelength of the TLCR5800. The output current of this photo-diode will be amplified with a trans-impedance amplifier circuit. The amplifier that will be used is the LMC6484 which is well suited for the amplification of relatively low input currents.

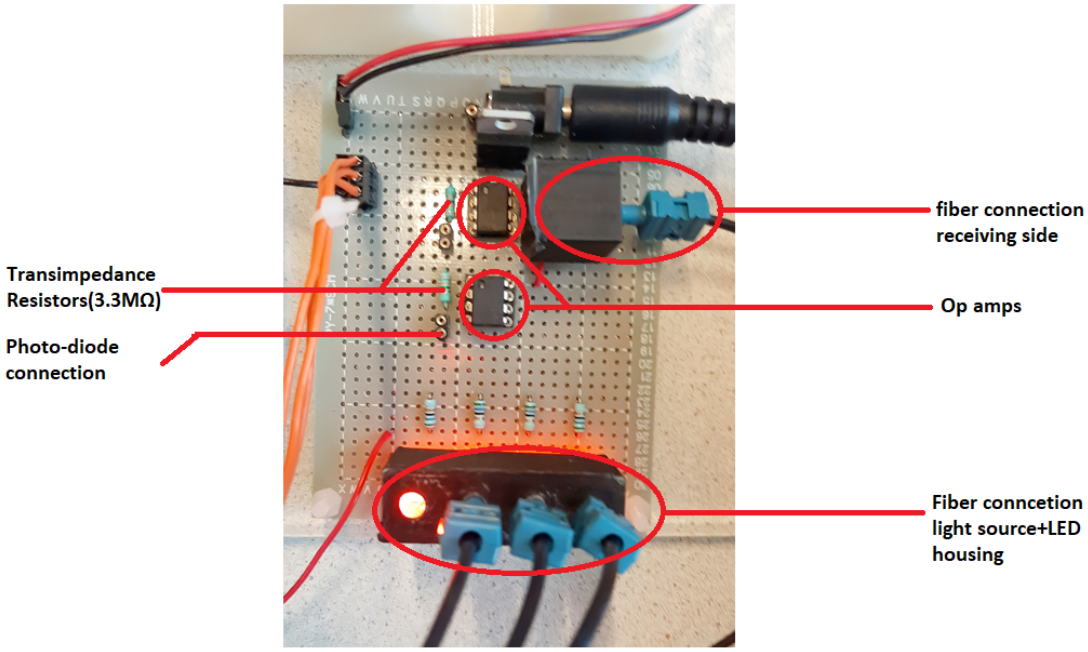

Figure 3.3: Picture of the circuit to send and detect light trough optical cables.

In figure 3.3 a picture can be seen of the circuit that allows to send light into an optical fiber with LEDs and detect the light on the receiving side with a photo-diode and trans-impedance amplifier. The outputs of the trans-impedance amplifiers are connected to the analog pins of an Arduino UNO. The op-amps are powered with 5V such that the output of the trans impedance amplifier clips at 5v and the signal to the analog pins of the Arduino do not exceed 5V.

3.4 Encoding Signal

To predict the shape of the signal as a function of the traveled distance along the encoding pattern, it is assumed that the encoding pattern is shaped as a repeating pattern of squares with the same width as the diameter of the core-diameter of the optic fiber, and where the distance between the sqaures is equal to the width of the sqaures. Additionally, If one assumes that

the light intensity in the core of the fiber is homogeneously divided over the intersection of the core, the expected measured light intensity I_v as a function of the distance can be calculated by means of a convolution integral between a circle with a diameter of 1mm, described by $y_1(x)$, and a square of 1mmx1mm, described by $y_2(x)$:

$$y_1(x) = \frac{1}{2}\sqrt{\frac{1}{4} - x^2},$$
$$y_2(x) = \frac{1}{2}\text{rect}(x).$$

Such that the convolution between the two surfaces becomes,

$$I_v \sim 2\int_{\infty}^{\infty} y_1(u)\,y_2(u-x)\,du \tag{3.1}$$

$$= \begin{cases} \cos^{-1}\left(\frac{r-x}{r}\right) - \sqrt{|r^2-(r-x)^2|}(r-x) & \text{for} x < 2r \\ \pi r^2 - \cos^{-1}\left(\frac{r-(x-2r)}{r}\right) + \sqrt{|r^2-(r-(x-2r))^2|}(r-(x-2r)) & \text{for} x > 2r \end{cases} \tag{3.2}$$

When the optic fiber moves one period with respect to the encoding patter, where one period is equal to the distance between the beginning of one square in the encoding pattern to the beginning of the next, one would expect the signal to be similar to the graph in figure 3.4.

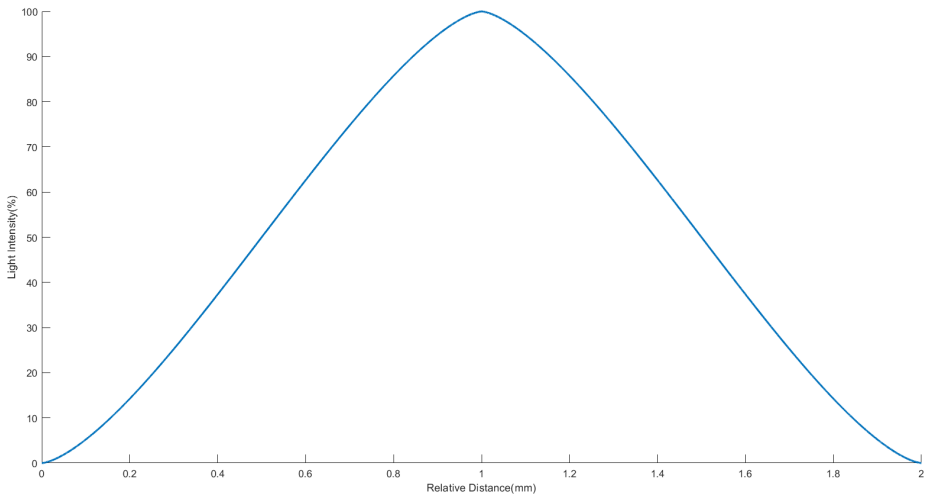

Figure 3.4: Expected signal according to equation 3.2

3.5 Design

In this chapter the designs of chapter three different designs are described, from which two designs are based on the same concept. The designs that are conceptually the same are described in the first two sections of this chapter. The second section, will treat a design that is an updated version of the design in the first section. This updated version is based on tests and the corresponding discussion, which is represented in section 4.1 and 5.1 respectively.

The basis of the two different designs will be elaborated. The designs will be based on the technical requirements mentioned in chapter 1:

- The encoder should be MR-safe.

- The encoder should have a resolution which is high enough to detect steps of 0.3mm from the pneumatic actuator.
- The precision of the encoder should be such that the encoder does not miss any steps.

To ensure that the designs are MR-safe, the designs will be fabricated with a 3d-printer. For this project the Objet 260 will be used. The designs will be mainly printed in the photopolymer called VeroWhite.

Since the resolution of the encoder should be such that steps of 0.3mm can be detected, the grating period corresponding to the encoding signal should be of a particular size, depending on several factors such as the desired resolution and the diameter of the optical fiber. It is also important that the grating structure of the design is not too small, since a too small grating may give problems while printing the design. Additionally, when selecting the dimension of the grating, the core diameter of the optic fiber should be taken into account. In order to have a periodic signal, which alternates from a fully blocked signal to a fully unblocked signal, the length of the grating period should at least be two times the core-diameter of the optical fiber. The core-diameter of the optic fiber is 1mm, which means that, ideally, the grating period should at least be 2mm. Thus an important objective of the designs is to enable a resolution of 0.3mm from a signal, or signals, that is/are periodic over a distance of 2mm. The fundamental difference between the two designs, that will be described in this section, is their approach to realize this objective. While realizing this, it should also be considered that the encoder should have a proper precision.

3.5.1 Rotary Encoder I

A method to detect steps of 0.3mm with an encoding pattern that repeats every 2mm can be achieved by translating the linear movement to an angular movement. A component that rotates proportionally to the linear movement of the motor, can transfer its angular movement to a wheel with a larger radius, such that the maximum encoding pattern size increases proportionally to the ratio between the radius of the first rotating component and the radius of the second rotating component.

In order to add a rotating component to the setup that moves along the setup simultaneously with the motor, the setup can be equipped with a linear spur gear rack, such that a spur gear can move along this rack. Figure 3.5 depicts a schematic of a teeth rack and a mating gear according to ISO standardized metric gearing. To this gear, a wheel will be attached with a larger diameter, engraved with a grating pattern.

In order to have an equal distance between each grating on the wheel, a full rotation of 360°should be divisible by the angular grating period τ, or $n = \frac{360}{\tau} \in \mathbb{N}$. Here the angular grating period is the angle that the gear has to rotate to complete a full period of the analog signal. The gear passes one pitch length p(see figure 3.5) on the rack for every teeth. If there are z teeth on the gear then for every gear-teeth $\frac{360}{z\tau}$ angular grating periods are completed. This means that for every angular grating period that has been completed, a linear distance of Δ was traveled where,

$$\Delta = \frac{zp\tau}{360^\circ} = \frac{zm\pi}{n}. \tag{3.3}$$

Here Δ is called the effective grating period. For this first design it is decided to detect steps upon events from one signal. This signal will be a digital signal obtained from applying a threshold to the analog signal arising from the grating and the optic fiber, which means that for every effective grating period there are two events, a rising and falling event. To have a resolution of at least 0.3mm, an effective grating period of 0.6mm is needed if only one signal is used to detect steps of 0.3mm. From section 2.5 it is clear however, that this grating period

could be doubled by using a combination of two signals with a phase-offset of 90° to realize the desired stepsize. Initially it will be decided to take one signal as reference to count the steps, and use the other signal, with a phase-offset of 90°, to determine the direction of the movement. This is done such that a possible error in the phase-offset between the two signals(e.g. due to an inaccuracy in fabrication), would not be a factor in the error of the stepsize. If it is demonstrated that the error in the phase-offset is not a significant factor, it can be decided in the next iteration to use the events of both signals to count the steps and double the effective grating period. Since the size p depends on the measure of $m = \frac{p}{\pi}$, and the value m only consists of a standard set of measures, the resolution cannot be chosen exactly $\Delta = 0.6mm$ if one chooses to conform to the standard set of ISO measures. However, as long as $\Delta < 0.6mm$, steps of 0.3mm will be detectable.

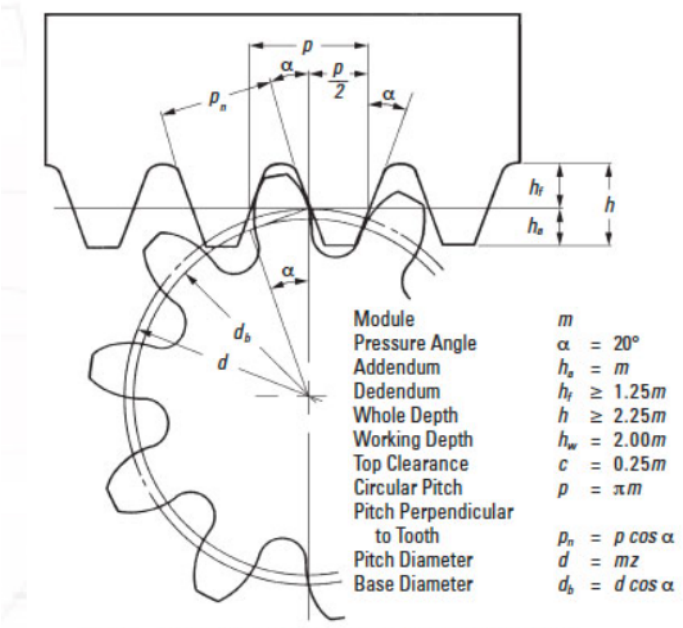

Figure 3.5: shows the tooth profile of a whole depth standard rack tooth and mating gear.[39]

To choose the m-size of the gear, the amount of teeth and the diameter of the wheel, the following aspects have to be taken into account:

1. Δ should be less than 0.3mm.
2. The dimensions of the gear and the wheel should be such that it can be implemented into the original design.
3. The dimensions of the gear should be such that the error due to 3d-printing will not affect the behaviour of the setup. This means that the teeth of the gear should not be chosen too small, since this would increase the relative error.

Proof of Concept

Before a design will be made with the required dimensions for implementation, a design will be tested that does not take into account point (2) such that there will not be any issues related to point (3). In this fashion, the concept can be proven, which is that steps of 0.3mm can be detected in both directions with the described method without considering the limitations of the dimensions. The base diameter d of the gear as depicted in figure 3.5 is equal to $d = mz$. Choosing $z = 10$ will result in a base diameter of around 10mm . When a gear is chosen with

$m = 1$, the circular pitch is $p = \pi m = \pi$mm. In order to have $\Delta \leq 0.6mm$ we first solve,

$$\frac{zp\tau}{360^\circ} = 0.6mm$$

for $z = 10$ and $p = \pi$, this results in $\tau \simeq 6.88^\circ$. This would come down to 52.35 grating periods in one revolution, however the amount of gratings per revolution should be a whole number. Therefore a the number of grating periods is chosen to be 55. To conform to the diameter of the optic fiber which is 1mm, the grating period on the wheel should be at least 2mm long. For a grating period of 2mm, the minimal required diameter of the wheel is $D = \frac{2 \cdot 55}{\pi} \simeq 35mm$

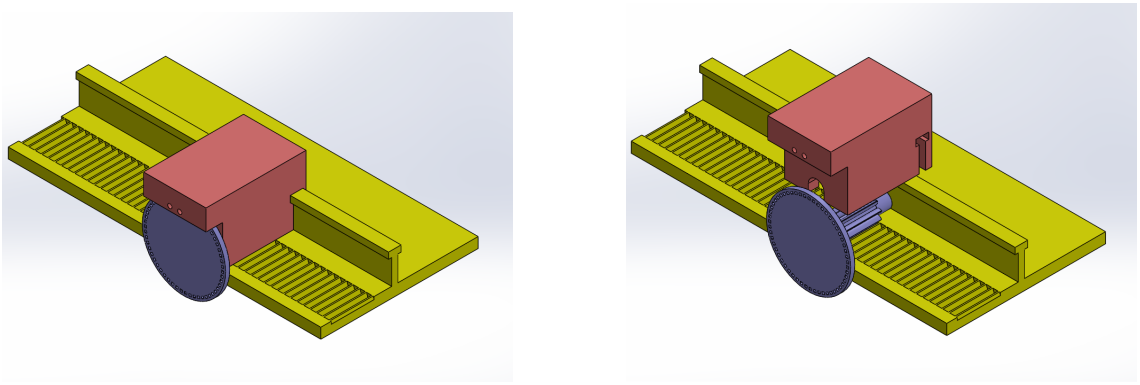

(a) Normal view **(b)** Exploded view

Figure 3.6: Cad model of the encoder concept, without pneumatic motor

The housing, in figure 3.6(red), has two holes so that the housing can be equipped with optical fibers. The holes are positioned such that the angle between the two lines from each hole to the midpoint of the wheel is 14.73°. This is because one angular grating period equals $360^\circ/55 \simeq 6.54^\circ$. To realize a quadrature signal with two periodic signals that have a relative phase-offset of 90°, the angle between the two holes should be $(n + 0.25) \cdot 6.54^\circ | n \in \mathbb{N}$. Taking $n = 1$ the angle between the holes approximately becomes equal to 14.73°.

3.6 Rotary Encoder II

Before proceeding with this section, the reader is advised to first read sections 4.1 and 5.1. In these section the testing and discussion of the previous design is treated, which forms the foundation of the design in this section.

Because it has been proven that steps of 0.3mm can be detected with the concept in the previous section, it is decided to integrate the next design into a simplified prototype of the total CathBot. This also means that the diameter of the wheel has to be decreased, such that it will fit inside the prototype. Furthermore adaptions will be made based on observations of the previous design to make the analog system more consistent.

The first observation mentioned at the end of the previous section, is that the surface of the wheel was moderately deformed and not completely flat. To prevent this, the wheel will be reinforced with extra material. The second observation was that the wheel moves back and forth along the rotation axis of the wheel, which may affect the consistency of the analog signal. To reduce this effect, the next design will have less spacing between the gear and the housing compared to the previous design. Lastly, the height of the grating pattern is exactly equal to the core-diameter of the fiber. This height will be doubled such that a small displacement of the wheel perpendicular to the axes of rotation will not affect the analog signal.

Since the error in the phase-offset is acceptable it is decided to use both analog signals to detect steps, which means that the effective grating period can be increased. This allows the grating

structure in the the wheel to be larger, or the diameter of the wheel to be smaller. In order to have a smaller diameter to make the dimensions of the design compatible with the dimensions of the CathBot, the M-size of the gear will be set from $M = 1$ to $M = 0.5$. In order give some oversight of the changes, the proposed changes for the next design are listed below.

- The m-size is set to $m = 0.5$
- Smaller diameter of the wheel
- Extra material to strengthen the wheel such that the effective radius does not change as much
- Height of grating holes in wheel are bigger
- Increase the effective grating period.
- The concept is integrated in a simplified version of the CathBot prototype with pneumatic motor.

For $m = 0.5$ the circular pitch p becomes $p = \pi m = 0.5\pi$. The amount of gear-teeth is again chosen to be $z = 10$. The effective grating period is not doubled but is made smaller than $\Delta = 1.2$mm to prevent that the maximum error of the resolution plus the nominal resolution does not exceed 0.3mm. Choosing an angular grating period of 20° gives, according to equation 3.3, an effective grating period of $\Delta = 0.8726646mm$. When using both analog signals with a relative phase-offset of 90°, this comes down to a resolution of approximately $\frac{\Delta}{4} = 0.2182mm$.

In figure 3.7 the complete CAD-model of the simplified version of the secondary part from the CathBot can be seen. The design is reduced to the point where only those parts are left which are essential for one pneumatic stepper-motor. Furthermore the model is shorter than the original prototype. To the model, the spur-gear rack is added to allow the gear in the housing to rotate. It can also be seen that the encoder is integrated into the stepper-motor. In figure 3.8 a closer view of the encoder can be seen.

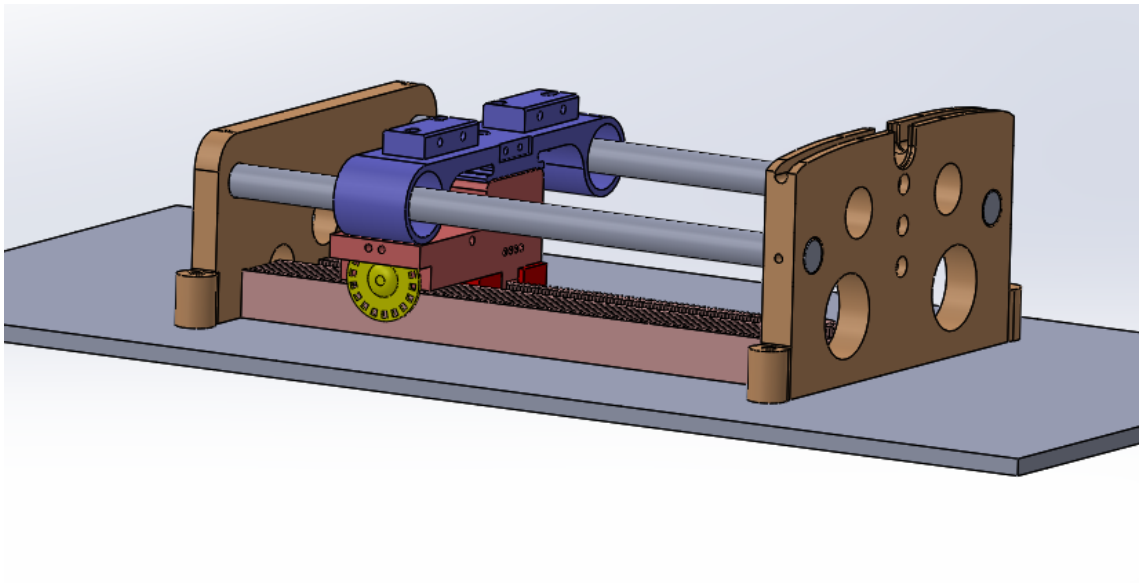

Figure 3.7: CAD-model of a simplified version of the secondary part from the CathBoth prototype.

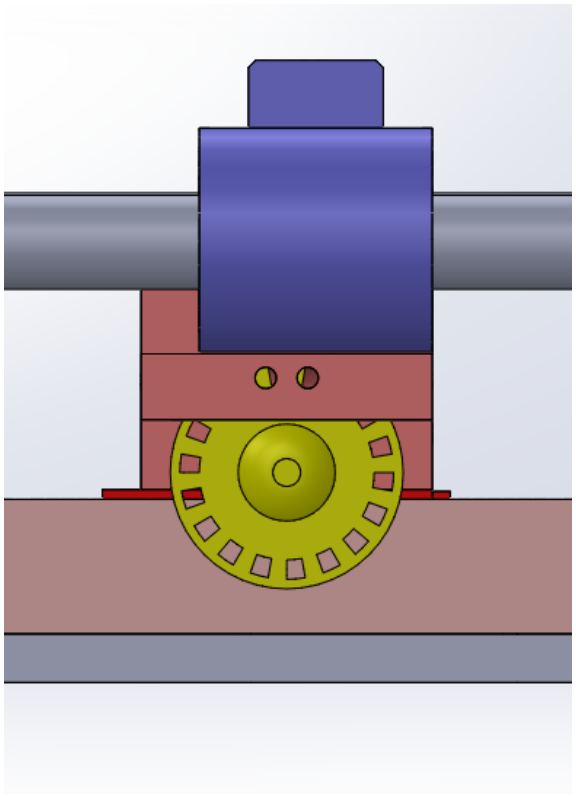

Figure 3.8: Front view of the encoder housing integrated in the pneumatic motor.

3.6.1 3-Phase Encoder

In the concept of the second design the plan is to create 3 analog signals corresponding to the movement of the motor over the rack(grey part figure 3.9). Three analog signals with a respective phase-offset of 120° are converted to a digital blockwave such that one grating period can be divided into six sections of equal length.

A digital block-wave with a duty cycle of 50% and a period of Δ has two events(rising and falling) equally divided over the period Δ. If there are n such block-waves with each a relative phase-offset of $\frac{360^\circ}{n}$, there are $2n$ events equally divided over the period Δ. Applying this to a linear encoder the resolution for n such signals and a grating period of Δ would then become $\frac{\Delta}{2n}$. So, to realize an encoder with a resolution of 0.3mm a grating period of $\Delta = 1.8mm$ is chosen with $n = 3$.

At the beginning of the section it was argued that the grating period should at least be 2 times the core-diameter(1mm) of the optical fiber to have a fully blocked signal for every period. Choosing $\Delta = 1.8mm$ will thus not result in a signal which is fully blocked for every period, nonetheless a periodic signal over Δ should still be convertible to a blockwave with a duty-cycle of 50%.

In order to create a grating period of $\Delta = 1.8$mm, a grating pattern is created in the rack with holes of a height of 2mm and a width=0.9mm repeating every 1.8mm, see figure 3.9. To create three digital signals which each have a relative offset of 120°, three analog signals have to be created relative to the movement of the motor. These analog signals will originate from optical fibers which are fixed in the holes in the caps(red part figure 3.9) of the pneumatic motor. The holes should have a relative distance of $(k + \Delta/3)$mm, where $k \in \mathbb{N}$ to realize the desired phase-offset.

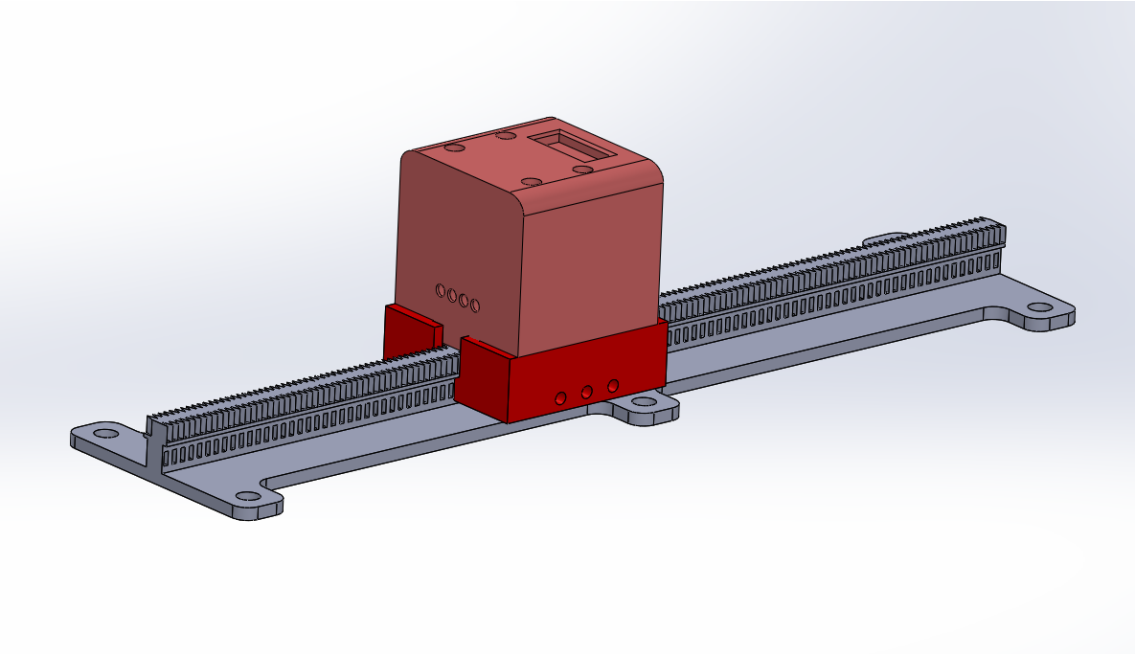

Figure 3.9: CAD model of the second design

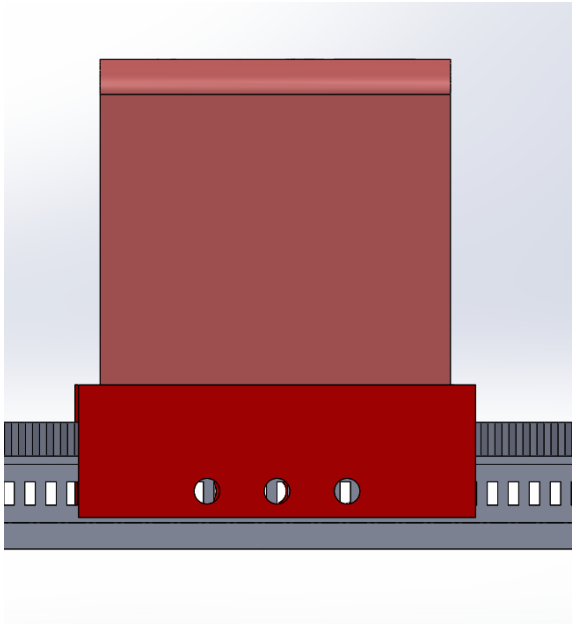

Figure 3.10: Front view of the second design

3.7 Test Setup

This section describes the methodology of testing the different designs. A large part of the testing will be done with an extra sensor to verify the distance that the motor-housing travels over the rack.

3.7.1 Rotary Encoder I

Before the concept will be developed further and will be linked to the pneumatic motors, the concept will be tested to verify that steps of 0.3mm can indeed be detected. In order to perform this test, a sensor will be attached to the housing of the test-setup that measures the relative

displacement of the housing(red part figure 3.6) with respect to the base(yellow part figure3.6). The sensor that will be used is the PAT9125EL optical tracking miniature chip, see figure 3.11.

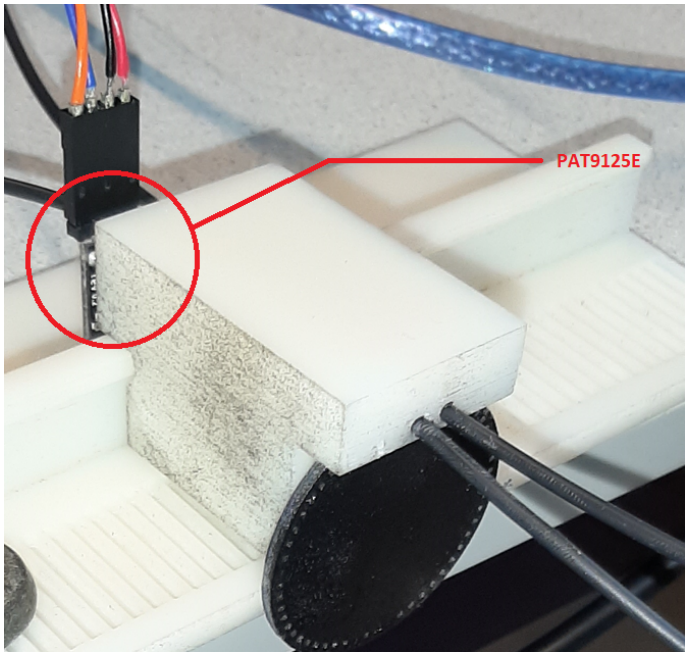

Figure 3.11: Picture of the test setup to test Rotary Encoder with Gear I

The sensor is calibrated by moving the gear-housing over the whole rack, which is a distance of 120mm, and count the amount of counted steps from the sensor. The two light signals from the optic fibers are converted to an electric signal between 0-5v, such that it can be read out by the analog input of the Arduino. The housing and the gear of the housing is moved along manually with an arbitrary velocity. A part of the analog signal is plotted against the measured distance from the PAT9125 in figure 4.1a.

3.7.2 3-Phase Linear Encoder

Two aspects of the design have to be tested to show that the concept, and the utilization of the concept, are sufficient to proceed with the design. Clearly the first aspect is that steps of 0.3mm are detectable. The second aspect is that the error of the measured stepsize with respect to the nominal stepsize is not too large.

As the previous design, this design will first be tested with a linear movement. Then, for one signal the ideal threshold will be determined, such that the standard deviation of the stepsize from this signal will be at its lowest. subsequently, the same thresholds will be applied to the other signals. Before applying this threshold to the remaining signals, it will be examined whether multiplying them with a scalar, has a positive effect on the standard deviation of the stepsize. The remaining signals will be transformed as follows with a_1 and a_2 as scalars:

$$S_2^* = (1 + a_1)S_2 \tag{3.4}$$

$$S_3^* = (1 + a_2)S_2 \tag{3.5}$$

After having determined the ideal threshold and scaling factors, the encoder will be tested together with the pneumatic motor. In figure 3.12 the test setup can be seen. The PAT9125 is connected to the base of the setup and a object is attached to the pneumatic motor such that the sensor tracks the movement of the motor.

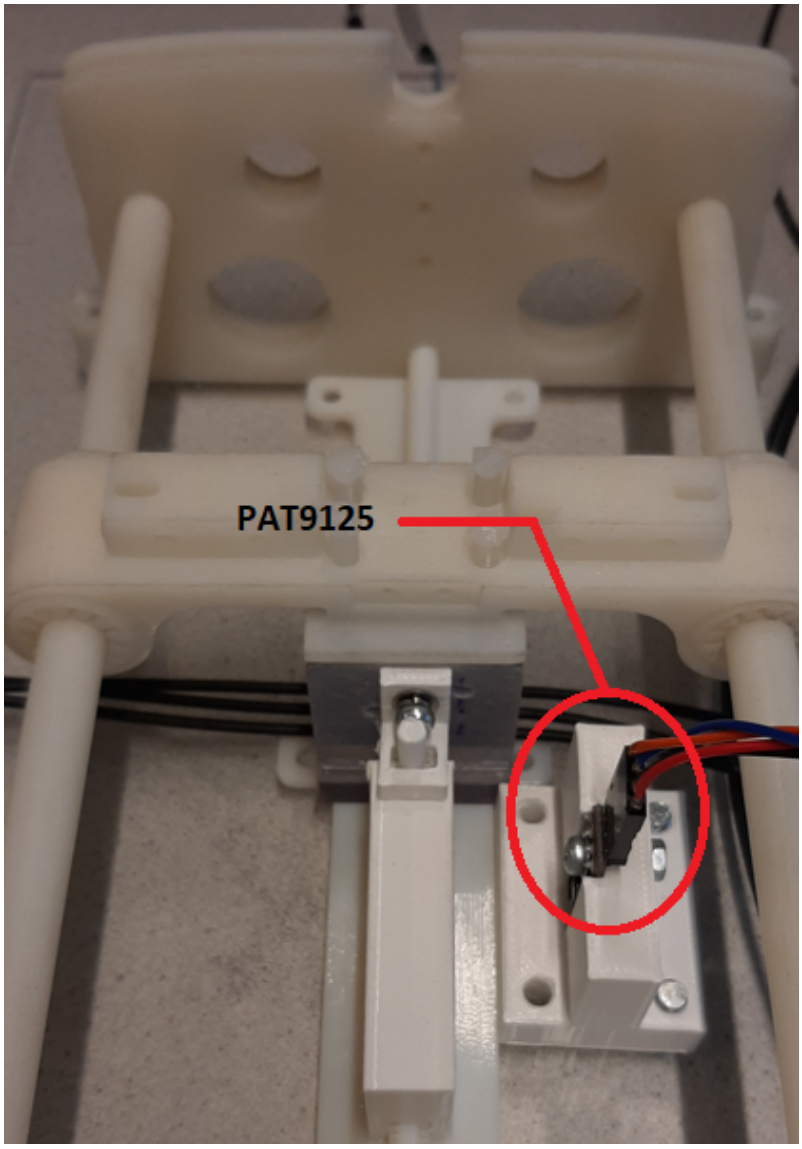

Figure 3.12: Test setup of linear encoder

4 Test Results

4.1 Rotary Encoder I

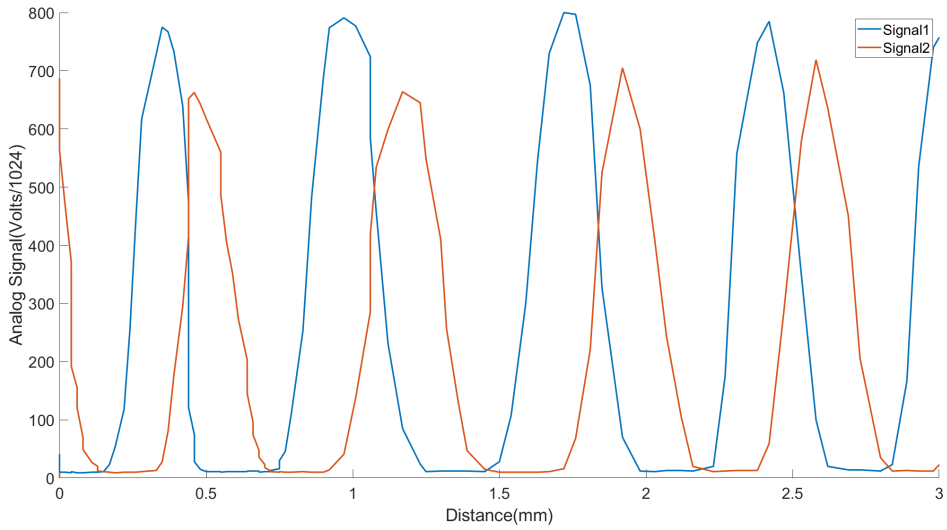

(a) Amplified signals from the photo-transistors

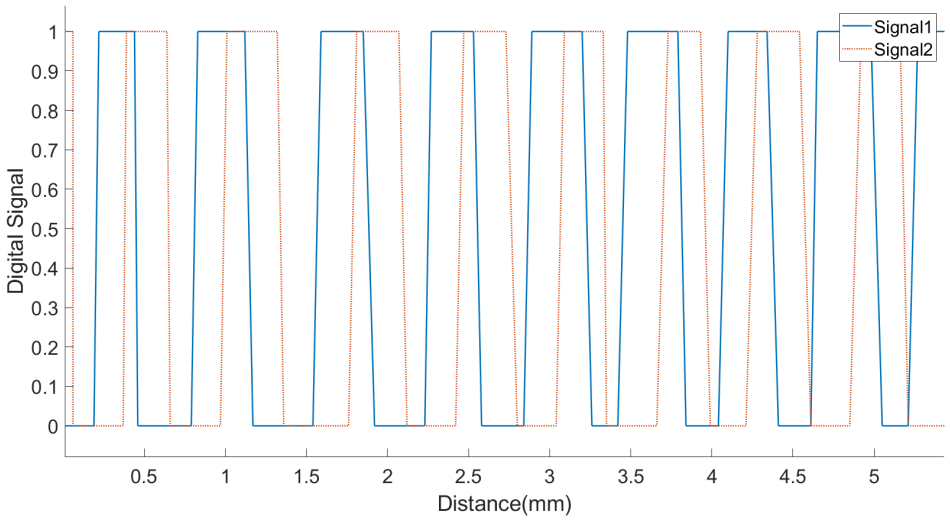

(b) Digital signals after applying a threshold to the analog signals

Figure 4.1: a)Analog signals from the encoder and b) corresponding digital signals

In figure figure 4.1a both analog signals can be seen for a, by the PAT9125E measured, total distance of 3mm. In order to detect steps of 0.3mm for one signal, a threshold will be applied such that the analog signal will be converted into a digital signal. This threshold has to be chosen such that the distance from a falling to rising event is equal to the distance from rising to falling event. If this would not be taken into consideration, the nominal resolution of the encoder would remain equal however the variation of the resolution would not be at its minimum. To choose a suitable threshold, different thresholds will be applied to a measurement over a distance of 15cm. For the different thresholds the average distance between falling to rising edge

and rising to falling edge will be plotted. In figure 4.2a and 4.2b these average values are plotted together with the standard deviation.

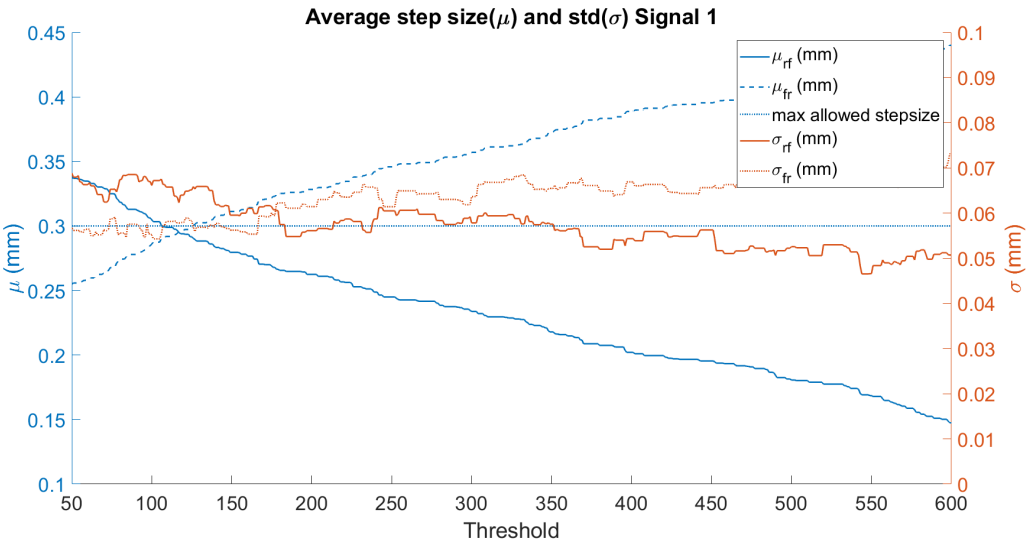

(a) Signal 1: Intersection of μ_{rf} and μ_{fr} at $\mu = 0.296$mm. The expected resolution is 0.286mm

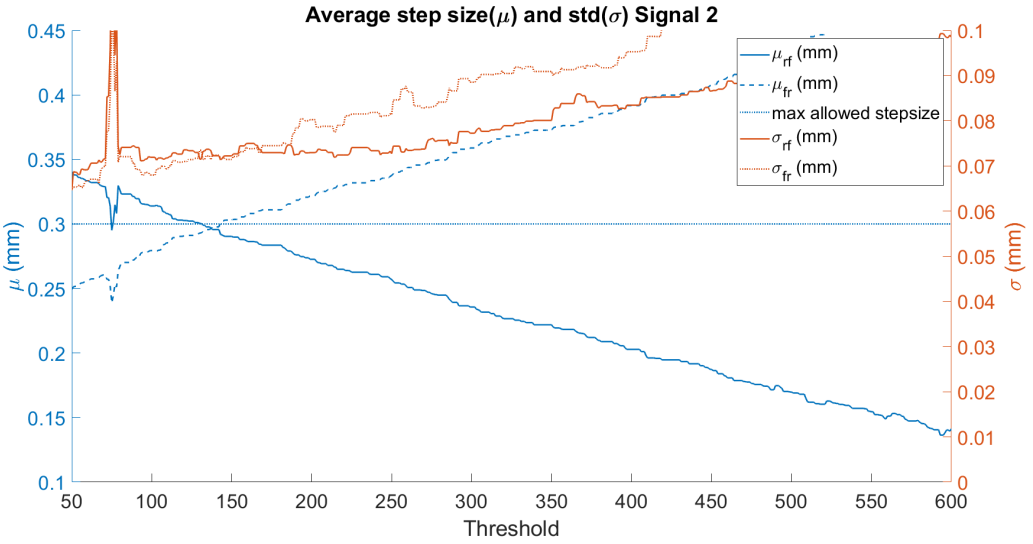

(b) Signal 2: Intersection of μ_{rf} and μ_{fr} at $\mu = 0.296$mm. The expected resolution is 0.286mm

Figure 4.2: Measured average (μ_{rf} average distance from rising to falling edge, μ_{fr} average distance from falling to rising edge.) And the corresponding standard deviations for different applying different thresholds.

Based on figure 4.2a and 4.2b the thresholds are chosen at a value of 115 and 136 respectively. Choosing the thresholds at these values results in the digital signal that can be seen in figure 4.1b. As mentioned before, one signal is used to count the steps, which is in this case signal 1 which has the lowest standard deviation. A test was done to compare the measured displacement by the encoder with the measured displacement by the PAT9125. The housing of the encoder was moved approximately with 3cm over the rack. The results of this comparison can be seen in figure 4.3. The error, which is defined as the difference between the displacement measured by the encoder and the displacement measured by the PAT9125 can be seen in figure 4.4. The mean absolute error was measured to be 0.165mm in this measurement. Furthermore, the average distance between rising/falling events of signal 1 and rising/falling events of signal

2, was 0.186mm. This is an average phase offset of 111.6° which is an error of 25% with respect to the desired offset of 90°.

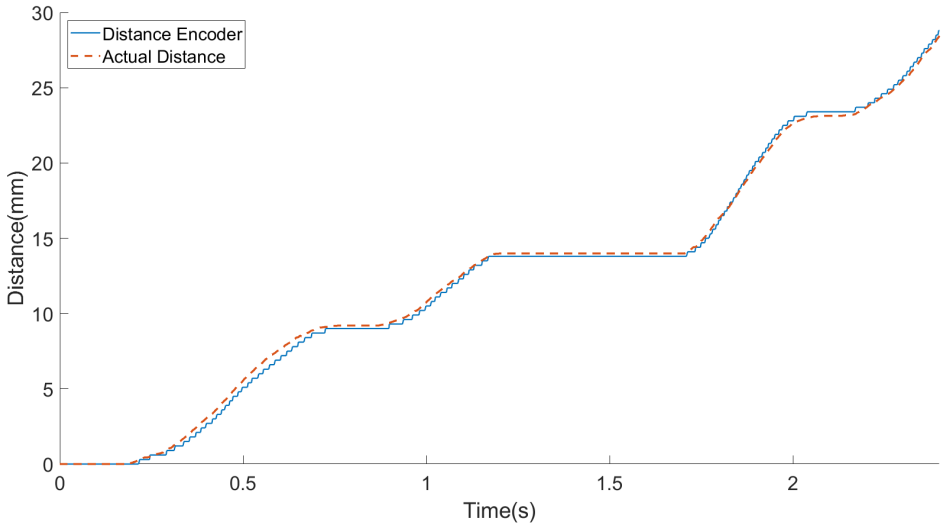

Figure 4.3: Analog signals of the encoder over a distance of 24mm. It can be seen that the amplitude varies significantly.

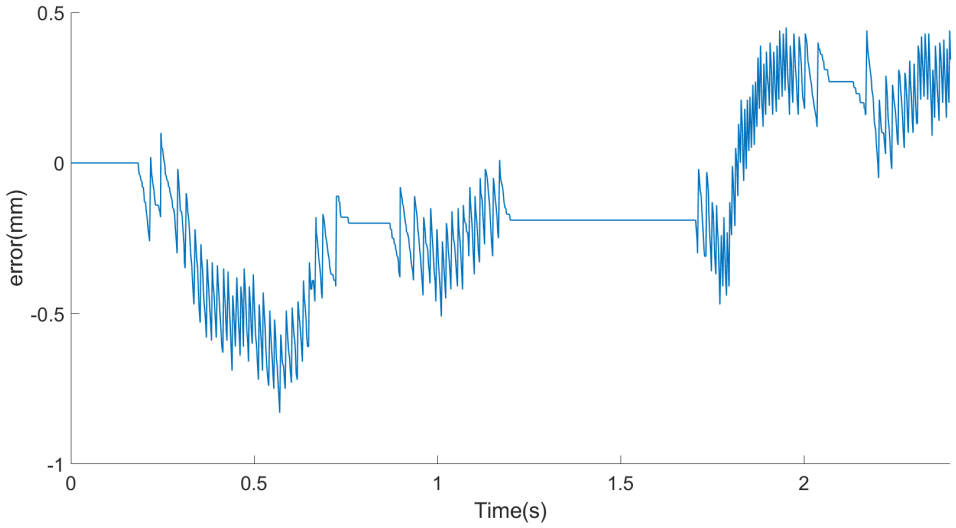

Figure 4.4: Difference between displacement measured by encoder and displacement measured by the PAT9125

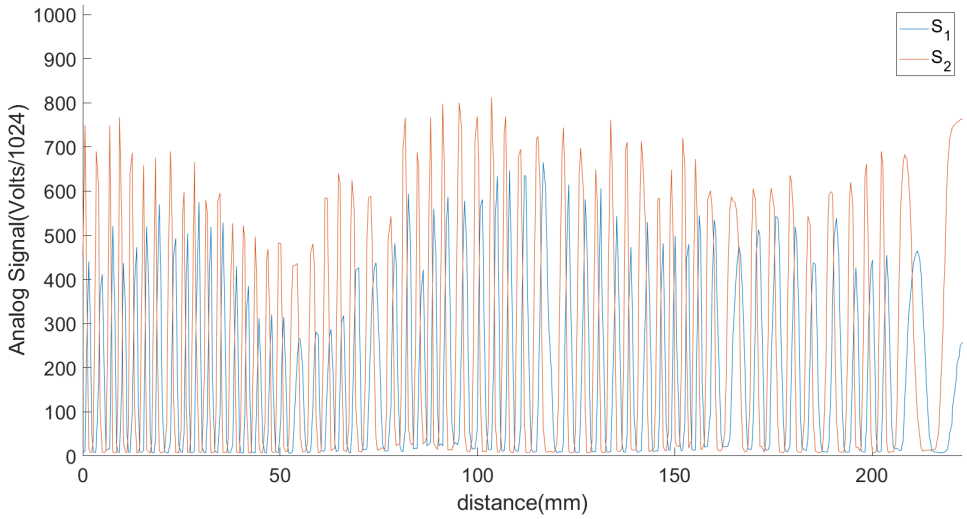

Figure 4.5: Analog signals of the encoder over a distance of 24mm. It can be seen that the amplitude varies significantly.

4.2 Rotary Encoder II

The analog signal of the rotary encoder with gear II can be seen in figure 4.6. The resulting analog signal of this design has a steeper change during the fluctuations. This corresponds to the smaller interruption-distance of the cable in the encoder. In figure 4.7 it is shown that the average stepsize exactly matches the expected resolution-stepsize of 0.2182mm for different thresholds. The standard deviation, which ranges from approximately 18% at a threshold of 300 to 33%of the resolution-stepsize at a threshold of 800.

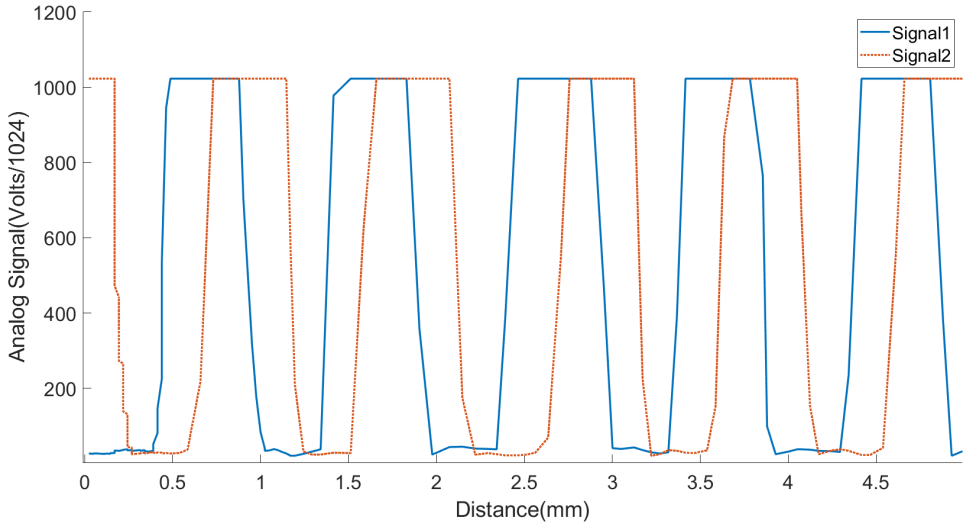

Figure 4.6: Analog signal 1 and 2 over a distance of 5mm during a continues movement

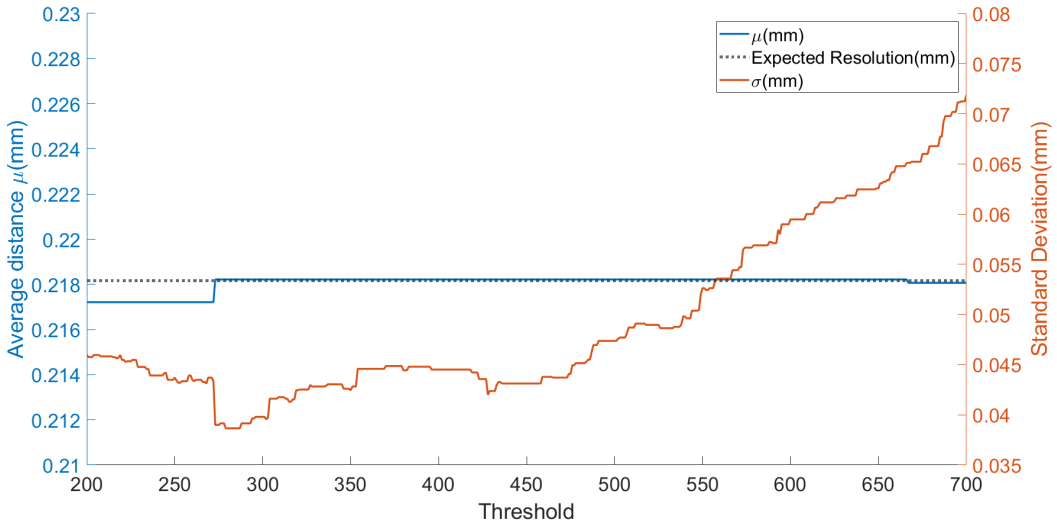

Figure 4.7: Average stepsize and the standard deviation of the stepsize for different thresholds. The standard deviation at a threshold of 300 is 18% of the average distance from event that threshold. The average phase shift between the two signals was 25.37%, or 91.33° of the effective grating period

After choosing a threshold of 300, the measured displacement of the encoder was compared to the measured distance of the PAT9125, see figure 4.8. The error is plotted in the next figure, and it is evident that the error becomes significant, which became already apparent from the previous figure. It can be seen that the encoder roughly tracks the movement of the housing of the pneumatic motor, however it occurs very frequently that in specific time frames the measurement of the encoder is inconsistent with the actual movement of the motor-housing.

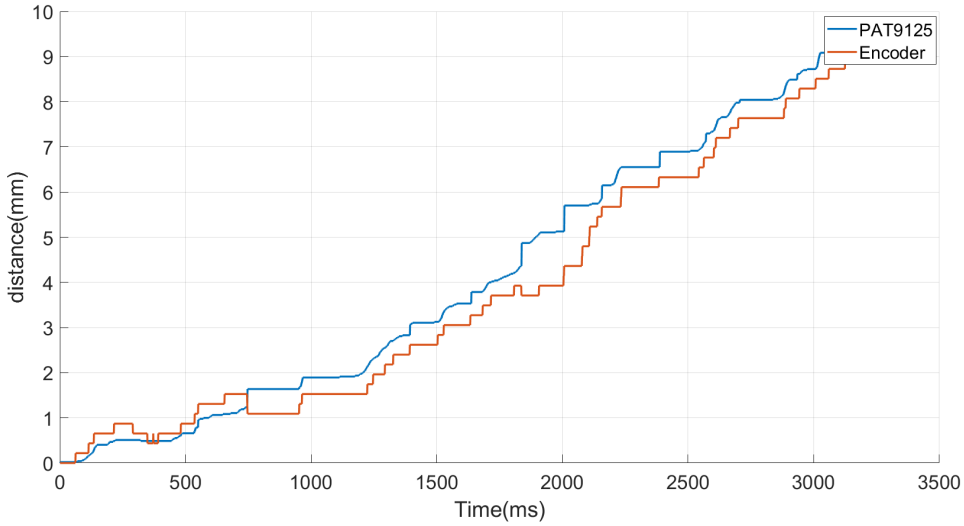

Figure 4.8: Displacement measured by the encoder, and displacement measured by the PAT9125 during a manually continues movement. The error of the encoder during this measurement is shown in figure 4.9

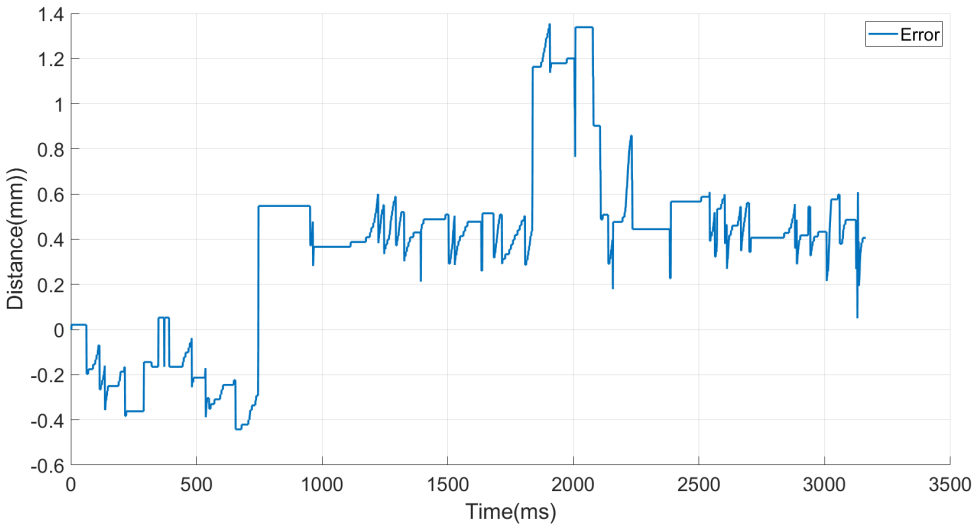

Figure 4.9: Difference between the measured distance by the PAT9125 and the measured distance of the encoder. The error increases when the traveled distance increases.

Next, the encoder was tested during movement with the pneumatic motor. The pneumatic motor moved with 8 steps/second. The displacement of the encoder was again compared with the PAT915, the result can be seen in figure 4.10. It is obvious that the measurement of the encoder is not consistent with the actual displacement. An analysis of the test result concluded that there are three causes for measurement errors, which are classified in three measurement complications. In figure 4.10 examples of these measurements complications, complication 1, 2 and 3(C1, C2 and C3), are encircled.

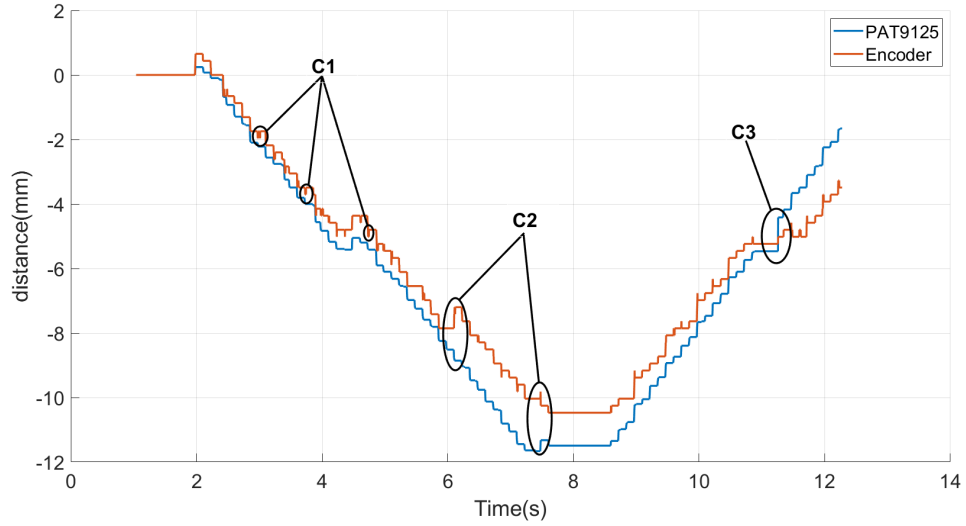

Figure 4.10: Plot of the measured displacement by the PAT9125 vs measured displacement by the encoder. During the test the pneumatic motor moved for an arbitrary distance with 8 steps per second. Clearly there is an inconstancy's between the two measurements. The inconsistencies are classified into three measurement complications which are discussed in section 5.2

4.3 Linear 3-phase Encoder

First the motor was moved continuously by hand. The analog signal corresponding to this movement can be seen in figure 4.11. Multiple measurements have been done, with a total

movement of 10cm, to determine the ideal threshold for signal 1. In figure 4.12 the average stepsize from event to event for different thresholds when applied to signal 1 can be seen. Also the standard deviation corresponding to this stepsize is shown.

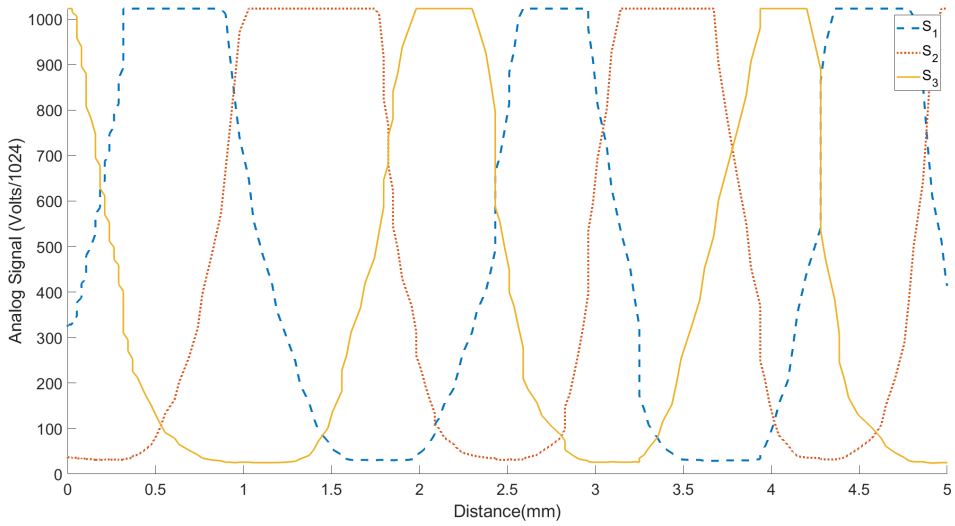

Figure 4.11: Analog signal of the 3-phase linear encoder during a continuous movement.

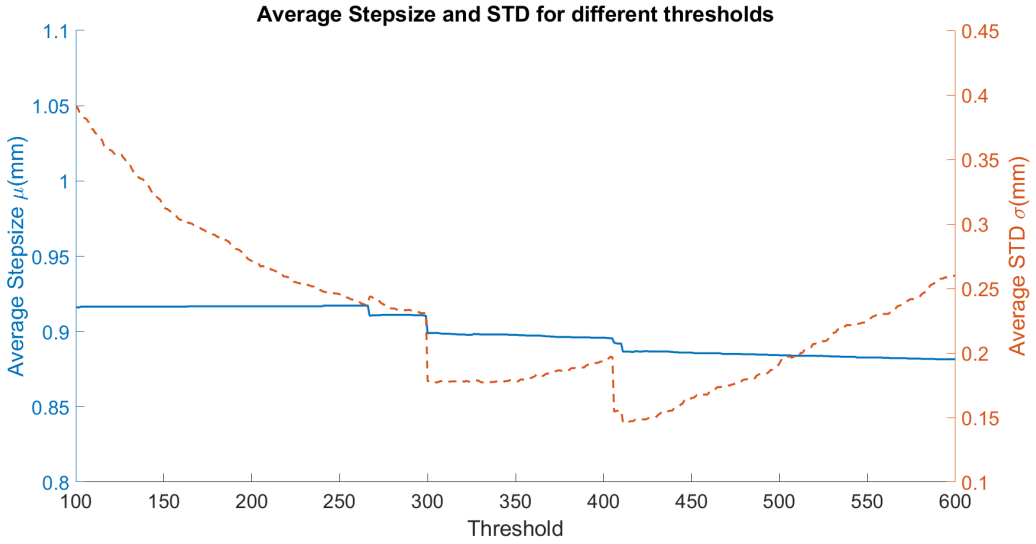

Figure 4.12: Average stepsize from event to event(blue) and the standard deviation of the stepsize(red) for signal 1

From figure 4.12 it can be seen that the ideal threshold lies somewhere between 400 and 450. After choosing a threshold of 400 signal 2 and signal 3 where transformed according to equations 2.1 and 2.2 for different values of a_1 and a_2. After applying this transformation, signal S_1 S_2^* and S_3^* where combined to create a 3-phase digital signal by applying a threshold of 400 to all of them. From this the average stepsize from event to event was measured and the standard deviation corresponding to all different values of a_1 and a_2. The standard deviations can be found in figure 4.13 and the average stepsizes in figure 4.14.

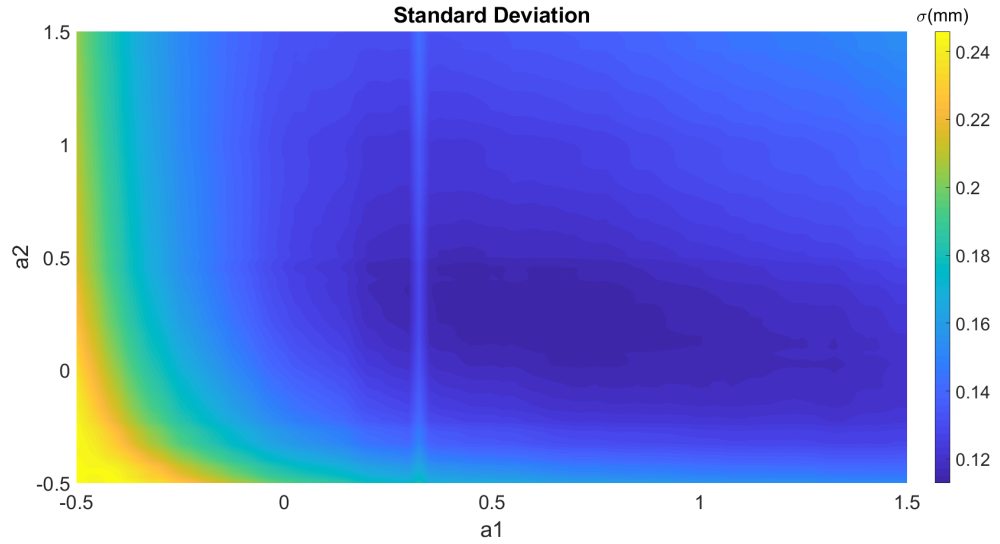

Figure 4.13: Standard deviation for different values of a_1 and a_2

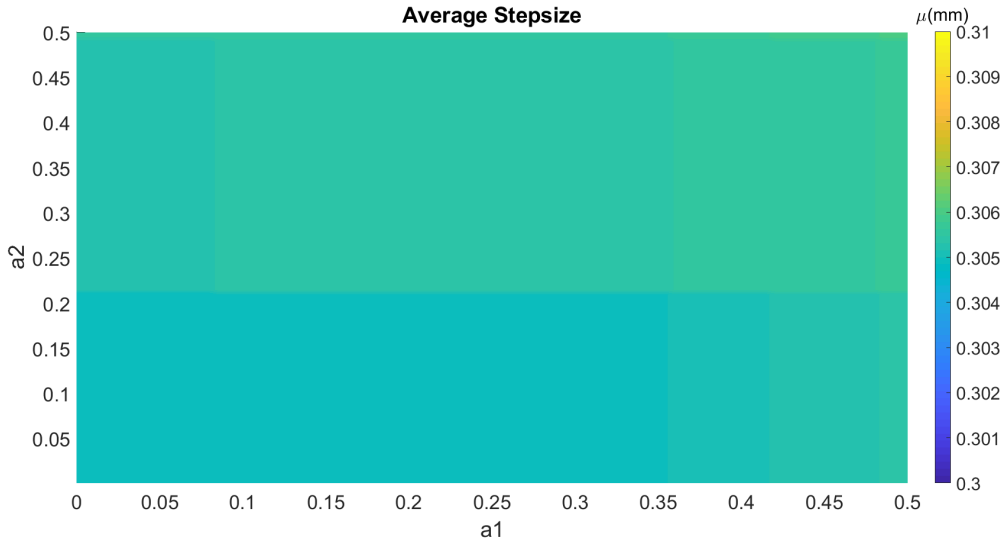

Figure 4.14: Average stepsize from event to event for different values of a_1 and a_2.

With a threshold of 400 and original signals S_2 and S_3 the distance was measured with an arbitrary movement and compared to the measurement of the PAT9125. The measurement can be seen in figure 4.15 together with the corresponding error in figure 4.17.

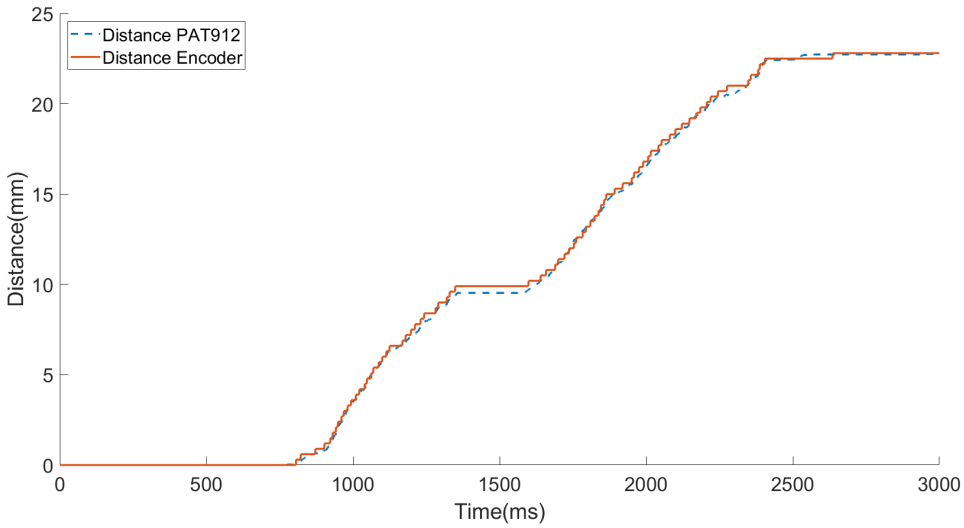

Figure 4.15: Measurement of the 3-phase linear encoder vs the measurement of the PAT

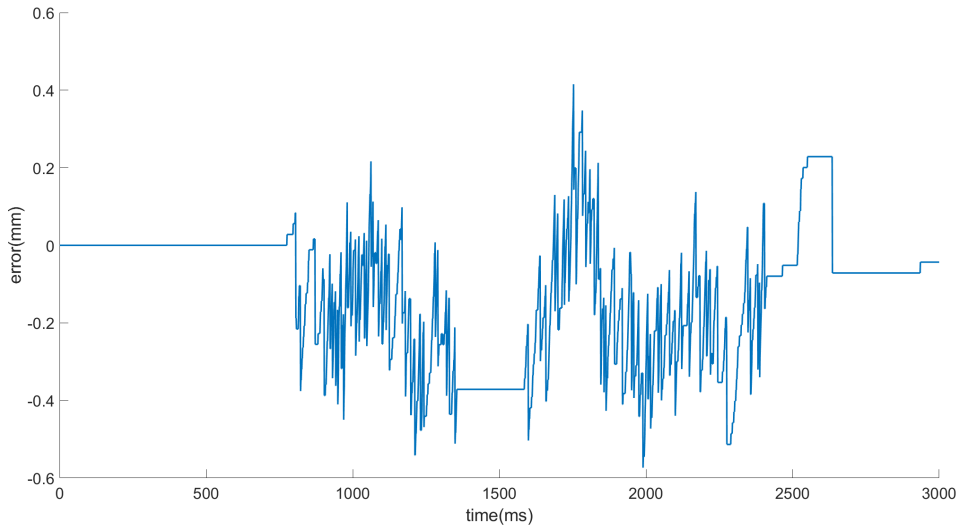

Figure 4.16: Error of encoder during continues movement of test from figure 4.15. The average absolute error was 0.17mm. The maximum magnitude of the error in the plot is 0.57mm.

Finally the encoder is tested with movement by the pneumatic motor. The motor moved with 2 steps per second. The measurement of the encoder vs the measurement of the PAT9125 can be seen in figure 4.17.

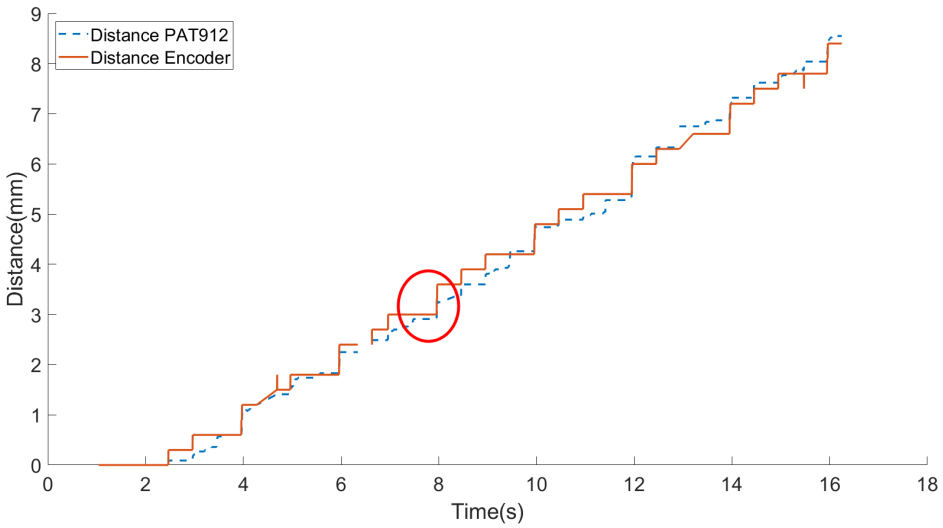

Figure 4.17: Test of the encoder with the pneumatic motor. Measurement of the PAT9125(blue) vs the measurement of the 3-phase linear encoder(red). The line depicts a measurement complication, where first a step is missed after which the measurement complication is corrected in the next step.

5 Discussion

5.1 Rotary Encoder I

The Rotary EncoderI was tested with a continues movement without pneumatic motor. From a sample in the analog signal in figure 4.1a it is apparent that the two signals do not have the same amplitude, and in addition each signal itself has an inconsistency in its periodicity since they are slightly different for each period. The inconsistency in the periodicity of the signals becomes even more apparent in figure 4.5, where the amplitude varies significantly. The inconsistency of the signal will very likely result in a lower precision when a constant threshold is applied. This is because the digital signal that is derived from the inconsistent analog signal with a constant threshold, will have a varying duty cycle in accordance with the variation of amplitude of the analog signal. This variation in the duty cycle implies a variation in the distance between the rising and falling events of the digital signal, which will cause a decrease in the precision of the encoder.

In this test it was shown that the accuracy was adequate since both averages, from rising to falling event and falling to rising event, μ_{rf} and μ_{fr}, intersect at 0.296mm in both signals in figure 4.2. This deviates with 3.64% from the expected resolution of 0.286mm, which can be attributed to an fabrication error during 3d-printing, or an error in the calibration of the PAT9125 sensor. The accuracy, with a deviation of 3.64% from the expected resolution, is sufficiently accurate since steps of 0.3mm from the pneumatic motor can still be detected with this deviation.

During the test the precision was measured represented as the standard deviation with respect to the average resolution for its corresponding threshold. At the intersection of μ_{rf} and μ_{fr} the average standard deviation($\frac{\sigma_{rf}+\sigma_{fr}}{2}$) for signal 1 is 20% of the resolution stepsize, and for signal 24% of the resolution stepsize.

After choosing the thresholds corresponding to the intersections in figure 4.2 a digital signal was generated, see figure 4.1b, which was used to track the distance of the motorhousing. As mentioned before, only one signal was used for distance tracking(signal1), and the other signal was only used to determine the direction of the movement. In the next design it can be decided to use the events of both signals to track the distance, however this will probably decrease the precision if the offset between the two signals is not accurate. In the test of this first prototype it was demonstrated that the offset deviated with 25% from the anticipated offset of 90°.

From the tracking of the distance in figure 4.3, it can be concluded that the concept can be used to track the distance of the motor housing, but does not have the required precision to be fully robust. As can be seen in the next figure the error during the continues movement was 0.83mm at its maximum. This is well over the resolution of 0.296mm which means that the error can not only attributed to the standard deviation of 20%. If one assumes that the encoder detects all grating periods that pass, and if it has detected N steps, one can conclude then that $N-1$ steps have been passed with absolute certainty. Whether the Nth step has indeed been finished by the housing of the motor is uncertain, since the standard deviation of the resolution is nonzero. From this reasoning the error can never be larger than the stepsize of the resolution plus the maximum deviation of an event with respect to the expected location of the event. That is, if one makes the assumption that the encoder detects indeed all gratings. Since it was proven during the measurement that a maximum error of 0.83mm exceeds the resolution stepsize plus ten times the standard deviation, it is very likely that the encoder occasionally misses grating periods since it would be unlikely that the maximum deviation of one event is greater than 10 times the standard variation.

An important issue which can be concluded from the test is that the amplitude of the analog signals varies too much. During the tracking of the distance it was necessary to hold the wheel

in a proper position to prevent a too large oscillation in the analog signal. The variation of the amplitude seemed to be periodic with respect to the displacement. This behaviour is possibly caused by the following observations:

- The wheel with grating pattern is not completely flat, which results in a varying effective radius, such that the grating pattern is not always exactly located between the optic fibers.
- During the movements of the wheel, the wheel moves slightly back and forth along the direction of its axle. Since the light that comes out of the optic fiber is slightly divergent, this may affect the consistency of the signal.
- The height of the grating pattern is exactly 1mm. A small change in the effective radius of the wheel may result in an inconsistency of the signal.

5.2 Rotary Encoder II

According to figure 4.7 the accuracy of the encoder exactly matched the accuracy of the 0.2182mm resolution that was anticipated on during the design. It should be noted however, that this is only the case when the encoder detects all gratings during the measurements. When the encoder misses gratings during a measurement, the detected analog signal does not match the true analog signal and the outcome of this particular measurement would not represent the quality of the true analog signal. Therefore, during this measurement it was ensured that only measurement samples would be taken where no gratings would be missed by the Arduino. However, it is certainly the case that gratings are frequently missed as will be shown later.

When one observes the shape of the analog signal in figure 4.6 it can be seen that the interval of a rising and falling event is much smaller than the interval of an event for the rotary encoder I. This is because the distance between the receiving and transmitting cable is reduced with respect to the previous design, and the current output of the photo-diode is still amplified with the same magnitude. One may expect that a smaller time interval for an event in the analog signal would have a positive effect on the precision. If one applies a threshold to the analog signal, the event in the digital signal is located somewhere on the time interval of the event in the analog signal. When this time interval decreases in size, the interval where the event in the digital signal is located will decrease which would possibly decrease the deviation of the true location of the event with respect to the designed location of the event. Interestingly, figure 4.7 shows that the standard deviation of the resolution has not significantly improved with respect to the standard deviation of the Rotary Encoder I. The standard deviation of the Rotary Encoder II ranges from 18% to 27% of the average resolution, as the standard deviation during the measurement of the Rotary Encoder I was 20% for signal 1 and 24% for signal 2. A difference between the measurements of both designs is that the precision of Rotary Encoder I was obtained by measuring the precision of the two signals apart, as the precision of Rotary Encoder II was obtained by combining the events of both signals. This could be an explanation for the observation that the precision of the Rotary Encoder II did not improve significantly for a smaller time interval of the events. However, measuring the precision of both signals apart did not improve the precision, which can be explained due to the fact that the average measured phase offset of the two signals was 91.33°. This is very close to the designed offset of 90°. Therefore, it can be concluded that combining the two signals of the Rotary Encoder II did not significantly affect the precision of the encoder.

In the next measurement the distance that the housing of the motor traveled over the rack was tracked with both the PAT9125 sensor and the encoder. It is assumed here that the distance tracked by the PAT9125 is the true distance, since the sensor was calibrated precisely before each measurement. In the graph of figure 4.8 it can be seen that the encoder roughly tracks the

movement of the housing, however there are serious deviations with respect to the movement of the housing in particular time intervals. The error(figure 4.9) is large enough to conclude, as it was concluded for the Rotary Encoder I, that the error can not be attributed only to a lack of precision, but it is very likely that the error should for a large part be attributed to the possibility that the Arduino skips crucial data from the analog signal.

The inconsistency with respect to the true movement of the motor also became apparent in the next measurement, where the encoder was tested in combination with an active pneumatic motor. In figure 4.10 the measurement of the encoder was compared to the actual movement of the motor, where the motor moved with 8 steps/second. Also during this measurement, the encoder roughly followed the movement, but again the measurement of the encoder deviated significantly for particular steps. The different inconsistencies in the measurements could be classified into three different classes, measurement complication 1, 2 and 3. Different examples of the measurement complications are encircled in figure 4.10.

When looking at the examples of measurement complication 1, it can be seen that when the pneumatic motor takes a step, the encoder initially responds by detecting a step, however the encoder gets back to its previous measurement value a few milliseconds later. In figure 5.1, the middle example of measurement complication 1 is enlarged to demonstrate this. In order to find the cause for this, the analog signal will be examined in this particular time-frame. In figure 5.2 the analog signal can be seen for the specific time frame of the C1-example in figure 5.1. It is evident that signal 2 changes from its maximum to its minimum around $t = 3.73s$. However, 3ms later the signal shoots back to a value in between the min and max which is slightly above the threshold. This causes the encoder to detect a step first, but resettling a few milliseconds after that. The encoder is, in this particular state, exactly between the state (11) and (00). This "in-between"-state falls exactly together with the end-begin of a step from the pneumatic motor.

From this a measurement complication 1 will be defined as follows: A step is not detected for the reason that between the start and end position of the motor of one step, there occurred no event in the analog signal. This means that the event that was supposed to be located between the start and end position of that motor-step, is located behind the end position of that step.

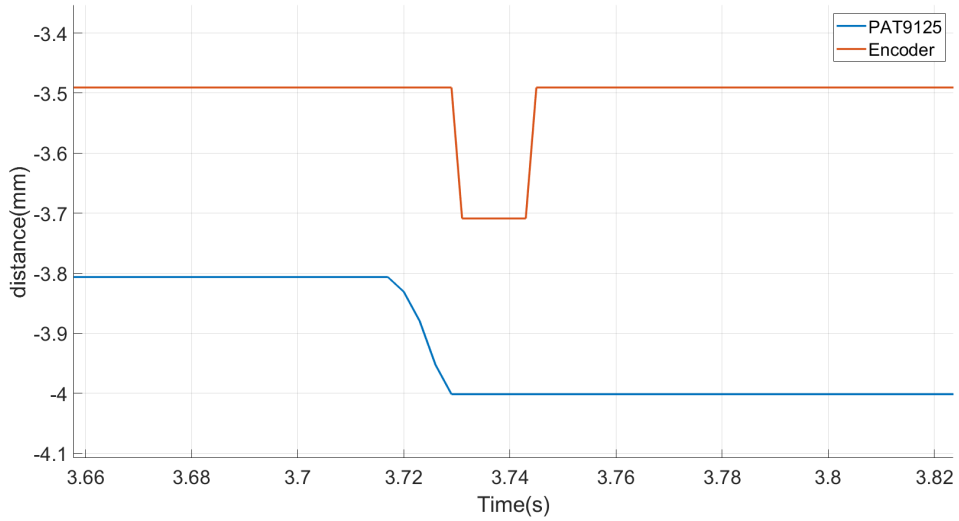

Figure 5.1: Distance measurement of the PAT9125 sensor and the distance measured by the encoder during the time frame of measurement complication 1.

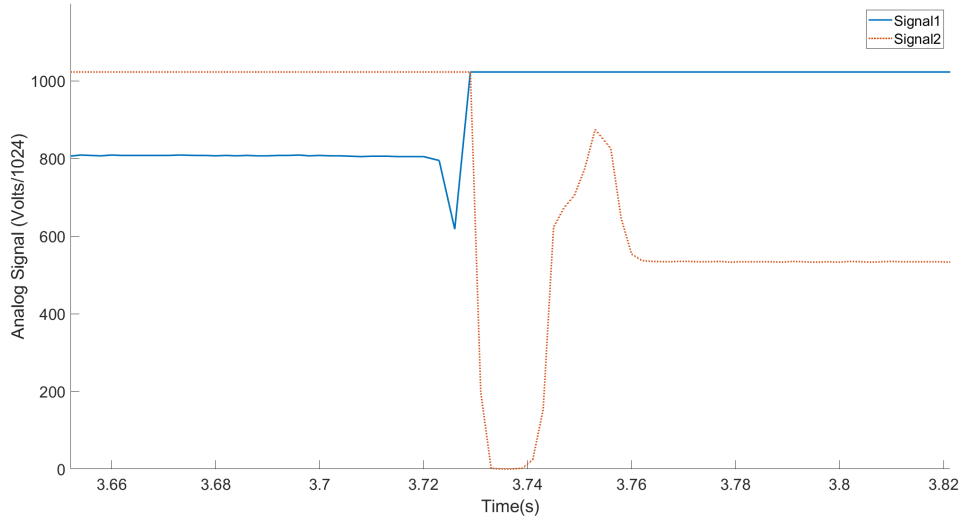

Figure 5.2: Analog signal for time frame of C1 example of figure 5.1

Next, measurement complication 2(C2) will be examined. In figure 4.10 two examples of C2 are encircled. These complications distinguish themselves in the sense that when the motor takes a step in a particular direction, the encoder interprets this as a movement in the other direction. To explain this, the first(or left)example of C2 in figure 4.10 will be examined.

At particular points the encoder seems to skip a step within the encoding signal. the correct order should be 00-01-11-10, however at moments it skips a step and goes e.g. from 11 to 00. At this moment it is impossible to tell which direction the motor has taken during that step, since there are two ways to go from 11 to 01 with two steps. Observing the encoder while the motor is making its steps it is noticed that at particular steps the motor housing moves slightly up, which causes the wheel in the housing to move slightly up and down because of the slack. This may be on of the causes an incoherence of the signal compared to the actual distance occurs. In figure 5.3a a close up view of measurement complication 2 of figure 4.10 can be seen. As the pneumatic motor takes a step in the negative direction, according to the sensor(PAT9125), the encoder interprets this as two steps in the other direction. To explain why the encoder interprets this as two steps in the opposite direction, a closer look is taken at the two analog signals in the same time interval in figure 5.3 and the encoder algorithm.

The digital signal, which is derived from the analog signal with a threshold of 500, has for distinct states: 11-01-00-10 respectively corresponding to step 0-1-2-3. In the encoder algorithm, the current step is defined as stp = $n+4i$, where n is the state between 0 and 3. When n goes from 0 to 3 we have $i = i-1$, if n goes from 3 to 0 we have $i = i+1$.

In figure 5.3a it can be seen that the state of the digital signal, for a threshold of 500, goes from 11 to 00 which corresponds to going from $n = 0$ to $n = 2$. In this particular time interval it is known from the sensor:PAT9125 that the motor moved in a negative direction according to the blue line in figure 5.3b. However, the algorithm does not interpret this as a negative movement, it simply interprets this as an immediate movement of 2 steps from state 0 to 2 in the positive direction, where state 1 was skipped. while actually the motor moved from state 0 to 2 where state 3 was skipped(so, 0-3-2 instead of 0-1-2). If state 3 would have been detected, the value i would have been decreased with 1, and the movement would indeed have been interpreted as two steps in the negative direction.

This particular measurement complication is thus derived from the fact that this encoder design will skip a step at times. This cannot be circumvented with an adjustment to the algorithm,

since their is no possibility to tell what the direction of the motor was if, according to the encoder, two steps are taken at once, simply because their are two ways of leaving and arriving at these particular states.

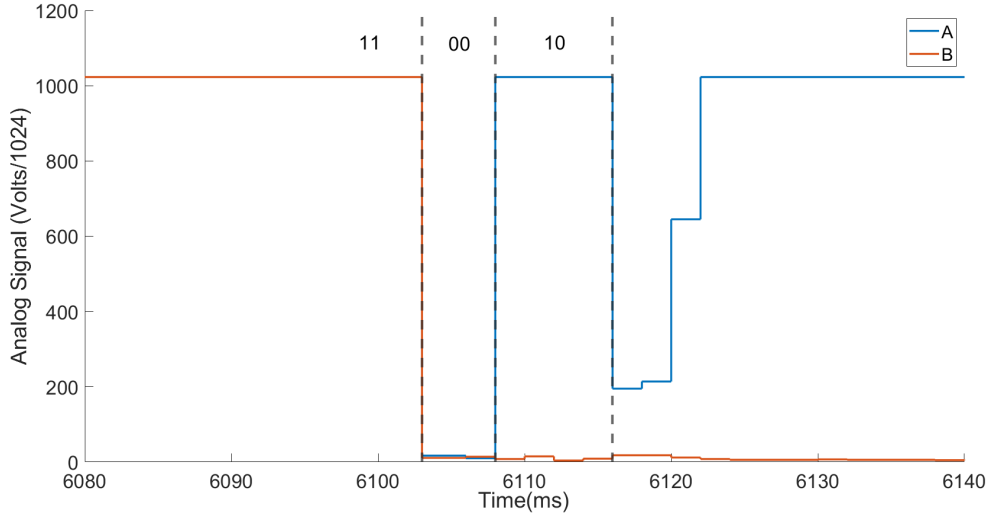

(a) Signal 1(A) and signal 2(B) zoomed in on time frame of measurement complication

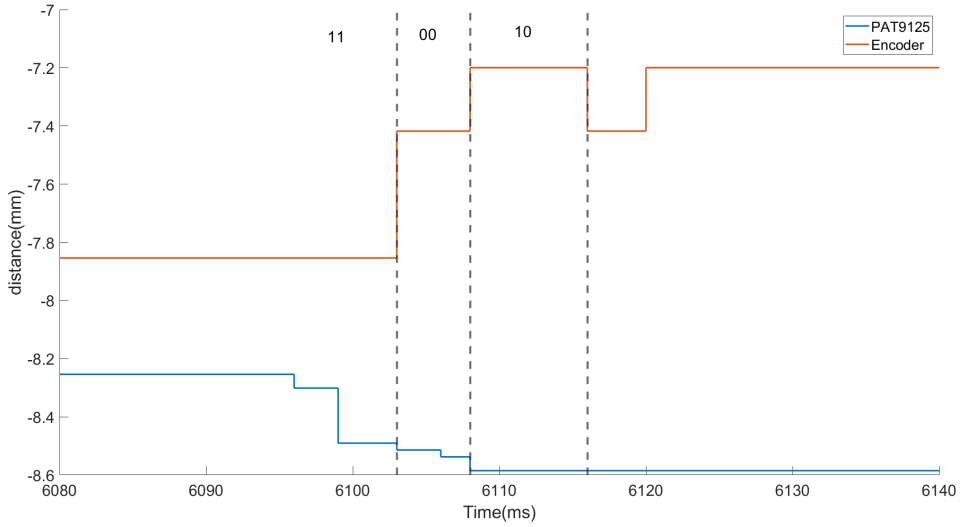

(b) Measurement complication 1

Figure 5.3: Cad model of the encoder concept, without pneumatic motor

The last measurement complication that was observed is measurement complication C3. Figure 5.4 shows the measurement complication can be seen more closely. 5.5 shows the according analog signals for the same time-interval. For an unknown reason, the motor takes a step of approximately 0.9mm at once, which is 3 times its nominal stepsize. It is assumed that there was a malfunction and the motor skipped a few steps. It can be noticed however that the encoder is completely inconsistent with this movement. It could be argued that the encoder missed a few steps while the pneumatic motor made a leap of 3 times its nominal stepdistance at once. However, the question would then be whether the encoder missed these steps "mechanically" so to say, or the encoder missed these steps because the movement was too fast for the Arduino. The average sampling fequency was 453Hz, which comes down to a sampling time of around 2.2 ms. From the data it was concluded that the large step measured by the PAT9125

was taken within one timeframe of 2ms. This may indicate that the arduino was not able to detect 3 events of the encoder, since the movement happened in one loop in the Arduino-code. The odd thing is then, that the encoder goes from state (11) to state(10) which indicates that, in the case that the motor did not take 1 step, the options left to go from state (11) to (10) is to take either three steps back, or to take five steps ahead.

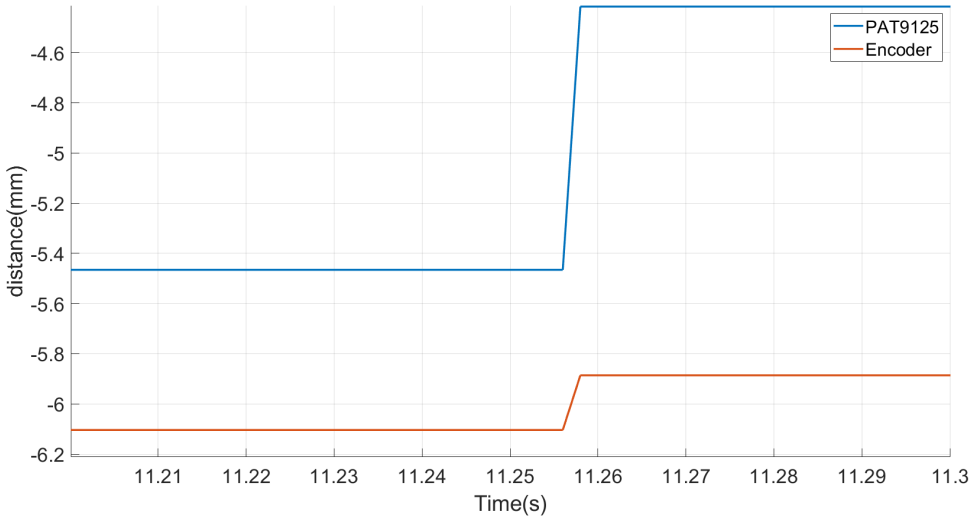

Figure 5.4: PAT9125 and encoder distance of figure 4.10 measurement complication 3

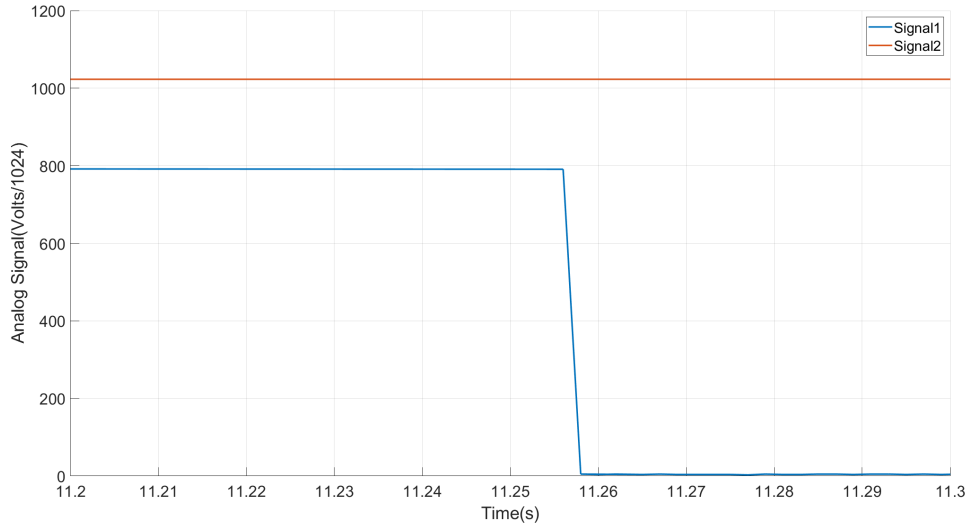

Figure 5.5: Analog signal on interval of measurement complication 3

It was also observed that the motor housing slightly rotates around its vertical axis during the movement of the motor. It was attempted to fix this by changing the material of the rods of the original design. In the first tests the rods were 3d-printed with VeroWhite. Later it was decided to use rods made out of fiber-glass, in order to have stiffer rods, and reduce the rotation. This ,however, affected the performance of the motor presumably due to a higher friction. This causes the encoder to deviate from the true position. A test was done to determine how much a maximum possible rotation corresponds to the measured distance because of this rotation. The test showed that a maximum rotation of the housing in the current setup can cause a de-

viation of 1.5 times the effective grating period, which comes down to a maximum deviation of 1.31 mm with respect to the true position of the motor.

5.3 3-Phase Linear Encoder

The second concept divided a grating period of 1.8mm into six sections by using three out of phase periodic signals. From the first figure in the results of the 3-Phase Linear Encoder it can be seen that the resulting analog signal is indeed a 3-phase signal with a respective phase-offset of which appears to be 120°. Additionally it can be seen that the 3 signals are not identical in shape which could cause the corresponding digital signals, after applying a threshold, not having the same duty cycle. Besides the fact that the three analog signals are not identical, it can be seen that each signal does not have an identical shape for each period. From the figure it can be concluded that the design manages to produce three periodic analog signals, however the appearing inconsistency together with a relative large time interval of the events of the signals will probably cause an undesired precision.

For signal 1, different thresholds are applied which results in plot 4.12 where the average stepsize from event to event is plotted together with the standard deviation. Different thresholds where applied to signal 1 in figure 4.12. The average stepsize from event to event lies around 0.9mm as expected. The standard deviation is between 17% and 22% of this stepsize for a threshold between 400 and 450. As mentioned in the results it was decided to choose a threshold of 400, as an ideal threshold was determined to be between 400 and 450 from figure 4.14. Since the three analog signals are not exactly identical as mentioned earlier, the remaining signals, signal 2 and signal 3, where first scaled with factors a_1 and a_2. Before scaling, it can be seen that the precision in terms of the standard deviation with respect to the resolution is 0.14mm or 46% with respect to the resolution. This precision is undesirable low, but the low precision was also anticipated based on the analog signal. Using signal 1 as reference, it was calculated that the average phase shift between signal 1 and signal 2, and between signal 1 and signal 3, combined deviated only 0.9% from the designed 120°. Therefore, it can be concluded that the low precision can be fully attributed to the shape of the analog signals.

In a attempt to improve the precision it was decided to transform signal 2 and signal 3 with respect to signal 1. Thereafter, the same the same threshold of 400 was used. It can be seen that the scaling can have a positive effect on the standard deviation, which can be brought down to approximately 0.12mm or 40% of the stepsize, compared to a standard variation of 46% when no scaling is applied.

Next, the encoder was tested with a continues movement. It can be seen that the encoder indeed tracks the movement of the motor, however there are significant deviations. In the next figure, the error during this measurement can be seen. The maximum magnitude of the error during the measurement was 0.57mm, which can be attributed to the relative low precision of the encoder. The precision in terms of the standard deviation was 0.14mm without scaling. By applying a normal distribution calculation, the probability that an error of this magnitude occurs is roughly 3%. One would expect however, that the mean of the error would be closer to zero if every inconsistency from the encoder would be the cause of the relative large standard deviation.

Finally, the encoder was tested with the pneumatic motor. The encoder seems to have no problems with the fast movements of the pneumatic motor. The small precision however, does form a problem in the detection of all the steps. Sometimes a step is taken by the pneumatic motor, but the encoder does not respond. It can be seen that this is often compensated in the next step of the motor, where in one stroke of the motor the encoder detects two steps. This is because the event of the digital signal, is not located between the start and endpoint of the motor, however the event lies between the next start and endpoint of the motor, often together with the next event. This causes the encoder to miss steps, and compensating it for the next motor

step. In figure 4.17 an example of this scenario is encircled. First the motor takes a step while the encoder does not detect anything. It has to be noticed that the motor takes a relative small step of 0.2mm instead of the nominal stepsize of 0.3mm. After this, when the motor takes the next step, the encoder detects two steps since two events lie between this start and endpoint of the motor.

Generally it can be concluded that the 3-Phase Linear encoder works satisfactory apart from the low precision. If one would examine this motor on robustness, in terms of predictive behaviour or consistent behaviour, it can be concluded that the encoder performs very consistent. There are no mechanical issues concerning implementation or undesired movement.

6 Conclusion

The aim of this project was to examine how an encoder could be developed for the CathBot. Two concepts were proposed to track the displacement of the linear pneumatic motor of the CathBot. Concept1: The Rotary Encoder) The linear movement of the motor was proportionally translated to an angular movement, which allowed for a larger grating structure. Concept 2:3-Phase Linear Encoder) A grating period of 1.8mm was divided into 6 sections 0.3mm by creating a 3-phase analog signal. In order to give answer to the research question of this project, the concepts were tested and evaluated on their precision, accuracy and robustness. Additionally a review was done on their lack of these qualities, and on possible solutions that would resolve these deficiencies, such that in future work a robust encoder for the CathBot can be developed.

When the designs are compared it can be concluded that the Rotary Encoder II and the 3-Phase Linear Encoder both were able to reproduce the designed accuracy. In terms of precision it can be said that the Rotary Encoder II performed significantly better than the 3-Phase Linear encoder. Defining the precision as the ratio between the standard deviation with respect to the resolution in percentage, the Rotary Encoder II had a maximum precision of 18%, whereas the 3-Phase Linear Encoder had a precision of 46% and 40% after scaling the analog signals. It is assumed that the precision of the Rotary Encoder II was higher because of the shape of the analog signal. However, in section 5.2 it was concluded that the precision did not improve when the interval time of the events in the analog signal would be decreased. Nonetheless, it should also be noted that this conclusion was drawn by a comparison between two designs of a different grating period. The Rotary Encoder I had an effective grating period of 0.296mm as the Rotary Encoder II had an effective grating period of 0.2182mm. It is not examined what the effect of the grating period size has on the precision. It may very well be that the precision, in terms of the ratio between the standard deviation and the resolution, decreases with an decreasing size of the grating period.

Comparing the designs regarding the robust behaviour, it can be said that the Rotary Encoder II had unreliable behaviour. This was because, as the housing of the motor turned around its vertical axis, the measurement by the encoder would be affected significantly. The effect of a maximum possible rotation of the housing along its vertical axis caused a deviation of 1.5 grating periods which is equivalent to approximately 1.31mm. This is a serious deficiency of the design compared to the 3-Phase Linear Encoder which had not such unreliable or unproductive behaviour. Additionally, the Rotary Encoder II had problems with fully detecting the analog signal. The the sampling frequency of the Arduino was 500Hz, however during particular fast movements of the motor multiple events occurred within a timeframe of 2ms. This caused the Arduino to miss events in the signal which resulted in invalid measurements.

Both designs had problems with measurement complication 2 mentioned in the discussion. This measurement complication occurred when an event of the analog signal is not located between the starting point and endpoint of the motor for one step. This could be attributed to three things. Firstly, the motor did not always take a step of 0.3mm, but there was always a slight deviation which causes intervals between the stationary locations of the motor which significantly differ in their distance. In such a manner, an interval of a motor-step may not fall together with an event of the encoding signal, and sometimes one motor-step interval may have two events, oftentimes after an interval with no events. Secondly, both designs had a significantly low precision which also contributes to the problem. Thirdly, during the design of both the rotary and linear encoder, the encoders where not aligned with the stationary locations of the motor such that the nominal location of the events where precisely in between the nominal locations of the static motor positions.

7 Recommendations

7.1 Rotary Encoder II

The sampling frequency that was used for the encoder design was approximately 500Hz, which was proven to be too low to ensure the detection of all encoder states. When the grating pattern moves too fast the encoder may miss encoder states. To resolve this the sampling frequency has to be increased. It is estimated that the sampling frequency should at least be doubled since it was shown that occasionally there occurred two changes of states(or events) during one sampling period. However, the two events are not necessarily evenly divided over the sampling period, thus the desired sampling frequency may very well be greater than two times the current sampling frequency. In order to increase the sampling frequency, an external A/D converter can be used such that interrupt handlers can be triggered on digital input pins.

The rotation of the motor housing during the movement of the motor creates a deviation of the linear position of the gear with respect to the center of the motor housing. In order to reduce this stiffer materials can be chosen for the rods of the original design. During the test the rods where 3d-printed with VeroWhite. A Stiffer material in the from of a glass-fiber pipe was tested, however this affected the performance of the motor.

7.2 3-Phase Linear Encoder

To main problem of the second design, which also occurred in the first design, was that it misses steps because the location of step detection is occasionally located just behind the end position of a motor step. In figure 7.1 a schematic can be seen which clarifies this. The figure depicts the ideal situation: The vertical black lines represent the position on one teeth pitch of 1.2mm where the motor is at a stationary position, and in between the vertical black lines the motor moves. So the motor takes steps from one vertical black line to the next vertical black line. The red vertical lines are the ideal positions where the encoder detects a step. When the described problem occurs during a measurement, the red line is positioned behind the correct black line instead of before, and at the next step this is corrected. This is depicted in figure 7.1b

First of all, the encoder should be properly aligned with the movement of the motor as depicted in figure 7.1a. This means that the average location of step detection should located in between the expected stationary locations of the motor. After that, the performance of the encoder depends on the behaviour of both the motor and the encoder itself. The stationary location of the motor is not always located on the exact designed location, which is every 0.3mm in this case. There is always a small error. To define the maximum allowed error of the encoder $\max(e_E)$, it is important to determine the maximum error of the motor $\max(e_m)$. Here, the error of the motor is thus defined as the distance that the motor deviates in static state, from its expected location in static state. If the average location of step detection is located between the expected stationary locations of the motors, then the maximum allowed error of the encoder becomes:

$$\max(e_E) < \frac{\text{stepsize} - \max(e_m)}{2}.$$

A method to reduce the maximum error of the encoder is to improve the quality of the analog signal. To enhance the quality of the analog signal, such that rising and falling events deviate less from their desired location, the event-interval where the analog signal chances its state, high->low or low->high, could be reduced, for example by using an optic fiber with a smaller diameter.

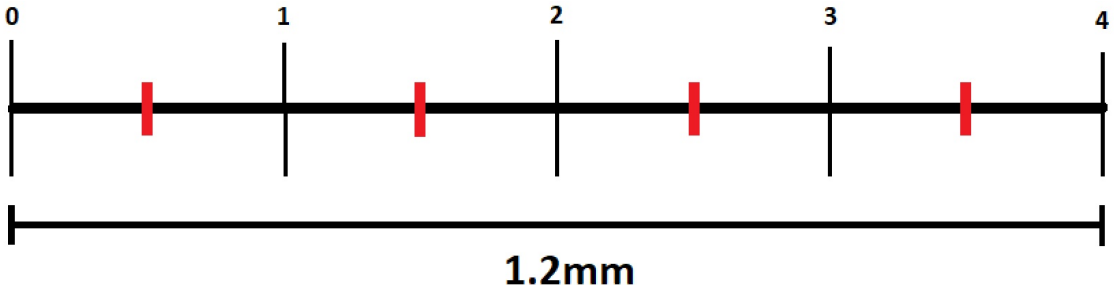

(a) The Vertical black lines are the positions on the teeth-pitch where the motor is stationary, so the motor moves from line to line. The red lines are the ideal nominal locations where the sensor detects a step. This is the ideal nominal location since it allows for a lower precision.

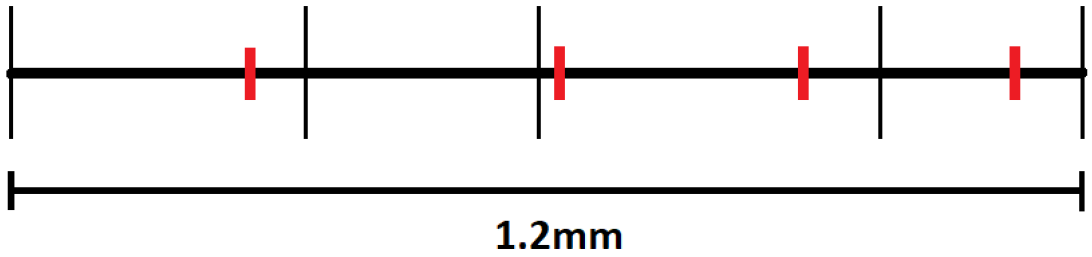

(b) In this schematic the lines represent the same as in the figure above. However, in this figure the steps of the motor are not exactly 0.3mm, and the encoder resolution is not always 0.3mm. This causes the encoder to miss steps.

Figure 7.1

A Naming of the parts of the designs

In this appendix chapter, the names in the figures refer directly to the correspodning Solidworks documents.

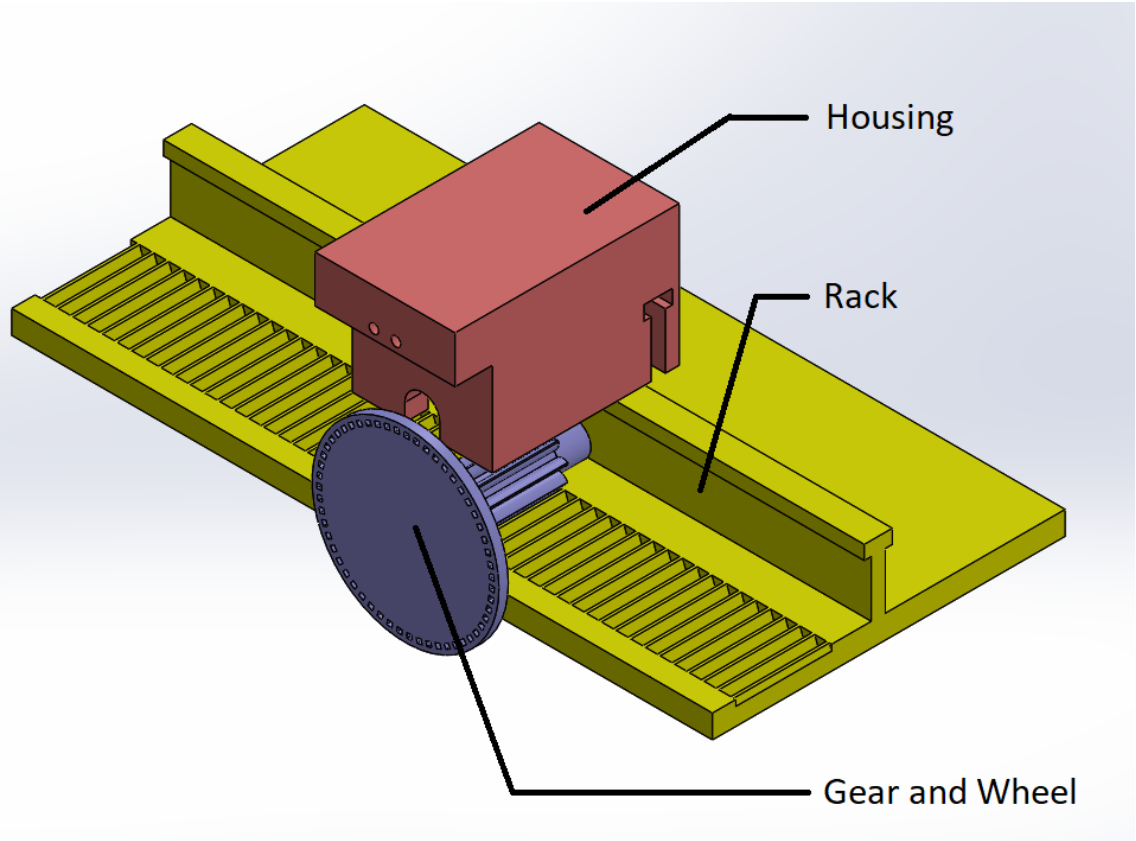

Figure A.1: Rotary Encoder I parts

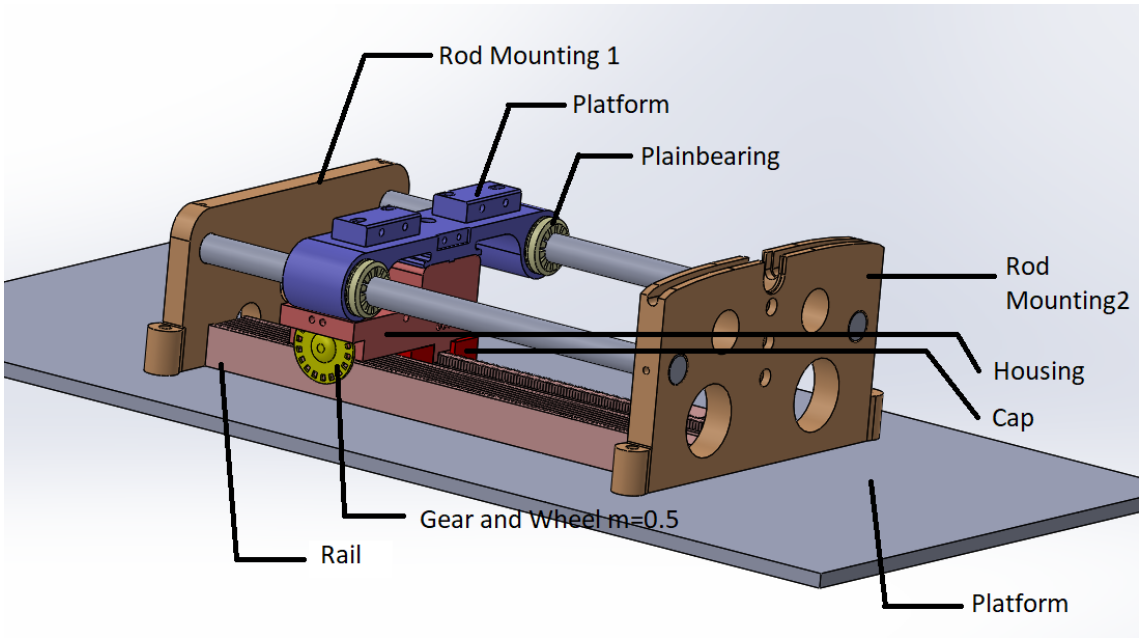

Figure A.2: Rotary Encoder II

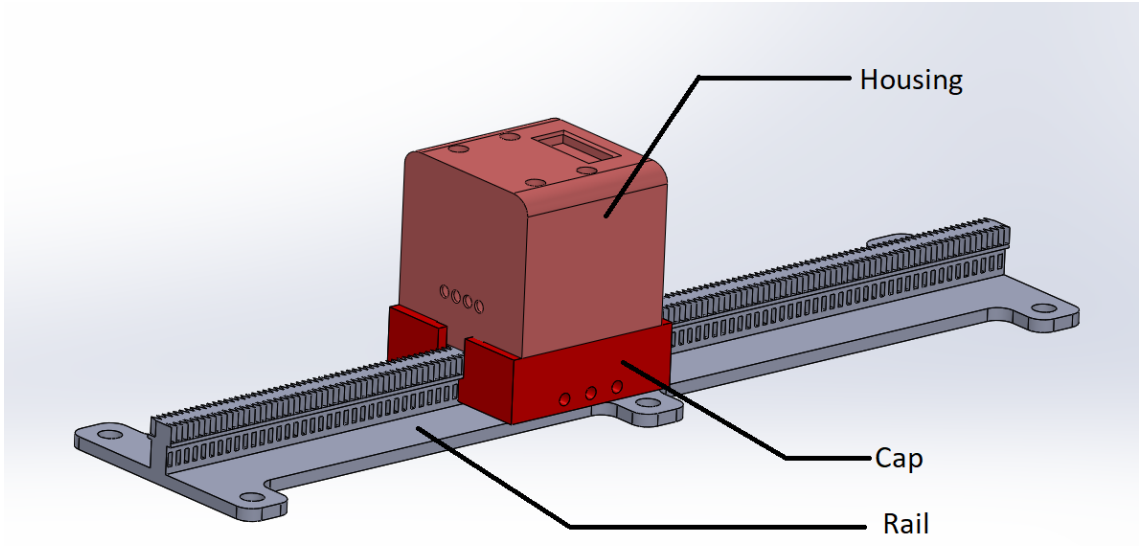

Figure A.3: 3-Phase Linear Encoder

Bibliography

[1] George A. Mensah et al. “Global Burden of Cardiovascular Diseases and Risk Factors, 1990–2019.” en. In: *Journal of the American College of Cardiology* 76.25 (Dec. 2020), pp. 2982–3021. ISSN: 07351097. DOI: 10.1016/j.jacc.2020.11.010. URL: https://linkinghub.elsevier.com/retrieve/pii/S0735109720377755 (visited on 06/09/2021).

[2] Hedyeh Rafii-Tari, Christopher Payne, and Guang-Zhong Yang. “Current and Emerging Robot-Assisted Endovascular Catheterization Technologies: A Review.” In: *Annals of biomedical engineering* 42 (Nov. 2013). DOI: 10.1007/s10439-013-0946-8.

[3] *PII: 0002-8703(95)90055-1 | Elsevier Enhanced Reader*. en. ISSN: 0002-8703. DOI: 10.1016/0002-8703(95)90055-1. URL: https://reader.elsevier.com/reader/sd/pii/0002870395900551?token=35B59AB20C68DD1F15F6F3714189838B4236530159F87E83D37B9F12115F8753CA12804A8167originRegion=eu-west-1&originCreation=20210614124027 (visited on 06/14/2021).

[4] Roman A. Hayda et al. “Radiation Exposure and Health Risks for Orthopaedic Surgeons.” en-US. In: *JAAOS - Journal of the American Academy of Orthopaedic Surgeons* 26.8 (Apr. 2018), pp. 268–277. ISSN: 1067-151X. DOI: 10.5435/JAAOS-D-16-00342. URL: https://journals.lww.com/jaaos/FullText/2018/04150/Radiation_Exposure_and_Health_Risks_for.2.aspx (visited on 11/28/2021).

[5] Tzu-Lung Ho et al. “Risk of cancer among cardiologists who frequently perform percutaneous coronary interventions: a population-based study.” eng. In: *European Journal of Clinical Investigation* 46.6 (June 2016), pp. 527–534. ISSN: 1365-2362. DOI: 10.1111/eci.12628.

[6] Luigi Di Biase et al. “Ablation of atrial fibrillation utilizing robotic catheter navigation in comparison to manual navigation and ablation: single-center experience.” eng. In: *Journal of Cardiovascular Electrophysiology* 20.12 (Dec. 2009), pp. 1328–1335. ISSN: 1540-8167. DOI: 10.1111/j.1540-8167.2009.01570.x.

[7] Mohamed E. M. K. Abdelaziz et al. “Toward a Versatile Robotic Platform for Fluoroscopy and MRI-Guided Endovascular Interventions: A Pre-Clinical Study.” In: *2019 IEEE/RSJ International Conference on Intelligent Robots and Systems (IROS)*. ISSN: 2153-0866. Nov. 2019, pp. 5411–5418. DOI: 10.1109/IROS40897.2019.8968237.

[8] William Insull. “The Pathology of Atherosclerosis: Plaque Development and Plaque Responses to Medical Treatment.” en. In: *The American Journal of Medicine*. Management of Atherosclerosis: A Practical Guide in 2008 122.1, Supplement (Jan. 2009), S3–S14. ISSN: 0002-9343. DOI: 10.1016/j.amjmed.2008.10.013. URL: https://www.sciencedirect.com/science/article/pii/S0002934308010176 (visited on 06/17/2021).

[9] Mushabbar Syed and Michael Lesch. “Coronary artery aneurysm: A review.” en. In: *Progress in Cardiovascular Diseases*. Percutaneous Treatment of Structural Heart Disease 40.1 (July 1997), pp. 77–84. ISSN: 0033-0620. DOI: 10.1016/S0033-0620(97)80024-2. URL: https://www.sciencedirect.com/science/article/pii/S0033062097800242 (visited on 06/18/2021).

[10] K-H Yiu and H-F Tse. “Hypertension and cardiac arrhythmias: a review of the epidemiology, pathophysiology and clinical implications.” en. In: *Journal of Human Hypertension* 22.6 (June 2008), pp. 380–388. ISSN: 0950-9240, 1476-5527. DOI: 10.1038/jhh.2008.10. URL: http://www.nature.com/articles/jhh200810 (visited on 11/25/2021).

[11] Thomas J. Fogarty and Rodney A. White. *Peripheral Endovascular Interventions*. en. Google-Books-ID: nERf58KlRkUC. Springer Science & Business Media, June 2010. ISBN: 978-1-4419-1387-6.

[12] Guang-Zhong Yang. “Devices for Endovascular Interventions.” In: ().

[13] Rob Mayfield- Hyperarts. *Department of Surgery - Endovascular Aneurysm Repair*. URL: https://surgery.ucsf.edu/conditions--procedures/endovascular-aneurysm-repair.aspx (visited on 12/06/2021).

[14] J. W. Hinnen et al. “Aneurysm Sac Pressure after EVAR: The Role of Endoleak.” en. In: *European Journal of Vascular and Endovascular Surgery* 34.4 (Oct. 2007), pp. 432–441. ISSN: 1078-5884. DOI: 10.1016/j.ejvs.2007.05.022. URL: https://www.sciencedirect.com/science/article/pii/S1078588407003991 (visited on 12/06/2021).

[15] Corine van Marrewijk et al. “Significance of endoleaks after endovascular repair of abdominal aortic aneurysms: The EUROSTAR experience.” en. In: *Journal of Vascular Surgery* 35.3 (Mar. 2002), pp. 461–473. ISSN: 0741-5214. DOI: 10.1067/mva.2002.118823. URL: https://www.sciencedirect.com/science/article/pii/S0741521402176919 (visited on 12/06/2021).

[16] Alan T. Hirsch. “Treatment of Peripheral Arterial Disease — Extending “Intervention” to “Therapeutic Choice”.” In: *New England Journal of Medicine* 354.18 (May 2006). Publisher: Massachusetts Medical Society _eprint: https://doi.org/10.1056/NEJMe068037, pp. 1944–1947. ISSN: 0028-4793. DOI: 10.1056/NEJMe068037. URL: https://doi.org/10.1056/NEJMe068037 (visited on 12/06/2021).

[17] Woong Yoon. “Embolic agents used for bronchial artery embolisation in massive haemoptysis.” en. In: *Expert Opinion on Pharmacotherapy* 5.2 (Feb. 2004), pp. 361–367. ISSN: 1465-6566, 1744-7666. DOI: 10.1517/14656566.5.2.361. URL: http://www.tandfonline.com/doi/full/10.1517/14656566.5.2.361 (visited on 12/06/2021).

[18] Song Jiang and Xiufen Xie. “Early interventional embolization in the treatment of cerebral aneurysm rupture.” In: *Pakistan Journal of Medical Sciences* 34.6 (2018), pp. 1463–1467. ISSN: 1682-024X. DOI: 10.12669/pjms.346.15786. URL: https://www.ncbi.nlm.nih.gov/pmc/articles/PMC6290242/ (visited on 12/06/2021).

[19] J. P. Joseph and K. Rajappan. “Radiofrequency ablation of cardiac arrhythmias: past, present and future.” en. In: *QJM* 105.4 (Apr. 2012), pp. 303–314. ISSN: 1460-2725, 1460-2393. DOI: 10.1093/qjmed/hcr189. URL: https://academic.oup.com/qjmed/article-lookup/doi/10.1093/qjmed/hcr189 (visited on 12/06/2021).

[20] Seyed Farokh Atashzar, Michael Naish, and Rajni V. Patel. “Active Sensorimotor Augmentation in Robotics-Assisted Surgical Systems.” In: *Mixed and Augmented Reality in Medicine*. Num Pages: 21. CRC Press, 2018. ISBN: 978-1-315-15770-2.

[21] Sarmad Mehrdad et al. “Review of Advanced Medical Telerobots.” en. In: *Applied Sciences* 11.1 (Jan. 2021). Number: 1 Publisher: Multidisciplinary Digital Publishing Institute, p. 209. DOI: 10.3390/app11010209. URL: https://www.mdpi.com/2076-3417/11/1/209 (visited on 11/25/2021).

[22] Kit-Hang Lee et al. “MR Safe Robotic Manipulator for MRI-Guided Intracardiac Catheterization.” In: *IEEE/ASME Transactions on Mechatronics* 23.2 (Apr. 2018). Conference Name: IEEE/ASME Transactions on Mechatronics, pp. 586–595. ISSN: 1941-014X. DOI: 10.1109/TMECH.2018.2801787.

[23] Pedro Moreira et al. “Tele-Operated MRI-Guided Needle Insertion for Prostate Interventions.” en. In: *Journal of Medical Robotics Research* 04.01 (Mar. 2019), p. 1842003. ISSN: 2424-905X, 2424-9068. DOI: 10.1142/S2424905X18420035. URL: https://www.worldscientific.com/doi/abs/10.1142/S2424905X18420035 (visited on 11/23/2021).

[24] Sunghwan Lim et al. “Robotically assisted long bone biopsy under MRI: cadaver study results.” en. In: *International Journal of Computer Assisted Radiology and Surgery* 14.1 (Jan. 2019), pp. 147–156. ISSN: 1861-6410, 1861-6429. DOI: 10.1007/s11548-018-1889-1. URL: http://link.springer.com/10.1007/s11548-018-1889-1 (visited on 11/23/2021).

[25] Dan Stoianovici et al. “Multi-Imager Compatible, MR Safe, Remote Center of Motion Needle-Guide Robot.” In: *IEEE Transactions on Biomedical Engineering* 65.1 (Jan. 2018). Conference Name: IEEE Transactions on Biomedical Engineering, pp. 165–177. ISSN: 1558-2531. DOI: 10.1109/TBME.2017.2697766.

[26] Dan Stoianovici et al. “A New Type of Motor: Pneumatic Step Motor.” In: *IEEE/ASME transactions on mechatronics : a joint publication of the IEEE Industrial Electronics Society and the ASME Dynamic Systems and Control Division* 12 (Feb. 2007), pp. 98–106. DOI: 10.1109/TMECH.2006.886258.

[27] Yili Fu et al. “Development of a novel robotic catheter system for endovascular minimally invasive surgery.” In: *The 2011 IEEE/ICME International Conference on Complex Medical Engineering*. May 2011, pp. 400–405. DOI: 10.1109/ICCME.2011.5876772.

[28] Sotiris Avgousti et al. “Medical telerobotic systems: current status and future trends.” en. In: *BioMedical Engineering OnLine* 15.1 (Dec. 2016), p. 96. ISSN: 1475-925X. DOI: 10.1186/s12938-016-0217-7. URL: http://biomedical-engineering-online.biomedcentral.com/articles/10.1186/s12938-016-0217-7 (visited on 11/23/2021).

[29] Dennis Kundrat et al. “An MR-Safe Endovascular Robotic Platform: Design, Control, and Ex-Vivo Evaluation.” eng. In: *IEEE transactions on bio-medical engineering* PP (Mar. 2021). ISSN: 1558-2531. DOI: 10.1109/TBME.2021.3065146.

[30] Vincent Groenhuis and Stefano Stramigioli. “Laser-Cutting Pneumatics.” In: *IEEE/ASME Transactions on Mechatronics* 21.3 (June 2016). Conference Name: IEEE/ASME Transactions on Mechatronics, pp. 1604–1611. ISSN: 1941-014X. DOI: 10.1109/TMECH.2015.2508100.

[31] Vincent Groenhuis and Stefano Stramigioli. “Rapid Prototyping High-Performance MR Safe Pneumatic Stepper Motors.” In: *IEEE/ASME Transactions on Mechatronics* 23.4 (Aug. 2018). Conference Name: IEEE/ASME Transactions on Mechatronics, pp. 1843–1853. ISSN: 1941-014X. DOI: 10.1109/TMECH.2018.2840682.

[32] Hung Van Hoang and Jae Wook Jeon. “Signal compensation and extraction of high resolution position for sinusoidal magnetic encoders.” In: *2007 International Conference on Control, Automation and Systems*. Oct. 2007, pp. 1368–1373. DOI: 10.1109/ICCAS.2007.4406551.

[33] Donatas Gurauskis, Artūras Kilikevičius, and Sergejus Borodinas. “Experimental Investigation of Linear Encoder’s Subdivisional Errors under Different Scanning Speeds.” en. In: *Applied Sciences* 10.5 (Jan. 2020). Number: 5 Publisher: Multidisciplinary Digital Publishing Institute, p. 1766. DOI: 10.3390/app10051766. URL: https://www.mdpi.com/2076-3417/10/5/1766 (visited on 10/29/2021).

[34] Mohieddine Benammar et al. “A Sinusoidal Encoder-to-Digital Converter Based on an Improved Tangent Method.” In: *IEEE Sensors Journal* 17.16 (Aug. 2017). Conference Name: IEEE Sensors Journal, pp. 5169–5179. ISSN: 1558-1748. DOI: 10.1109/JSEN.2017.2723619.

[35] A. Bunte and S. Beineke. “High-performance speed measurement by suppression of systematic resolver and encoder errors.” In: *IEEE Transactions on Industrial Electronics* 51.1 (Feb. 2004). Conference Name: IEEE Transactions on Industrial Electronics, pp. 49–53. ISSN: 1557-9948. DOI: 10.1109/TIE.2003.822084.

[36] Nobuhiko Hata, Ferenc A, and Ron Kikinis. “MR Compatible Surgical Assist Robot: System Integration and Preliminary Feasibility Study.” In: Nov. 2000. ISBN: 978-3-540-41189-5. DOI: 10.1007/978-3-540-40899-4_95.

[37] Roger Gassert et al. “Sensors for Applications in Magnetic Resonance Environments.” In: *IEEE/ASME Transactions on Mechatronics* 13.3 (June 2008). Conference Name: IEEE/ASME Transactions on Mechatronics, pp. 335–344. ISSN: 1941-014X. DOI: 10.1109/TMECH.2008.924113.

[38] Garland Best and Ömür M. Sezerman. “SHEDDING LIGHT ON HYBRID OPTICS: A Tutorial in Coupling.” EN. In: *Optics and Photonics News* 10.2 (Feb. 1999). Publisher: Optical Society of America, pp. 30–34. ISSN: 1541-3721. DOI: 10.1364/OPN.10.2.000030. URL: https://www.osapublishing.org/opn/abstract.cfm?uri=opn-10-2-30 (visited on 06/24/2021).

[39] *Elements of Metric Gear Technology*. URL: https://www.sdp-si.com/resources/elements-of-metric-gear-technology/.